이학박사학위논문

주변 국가들로부터 이동해 오는 대기오염물질이 한국의 대기질에 미치는 영향 연구

The influence of trans-boundary air pollutants from neighboring countries on the PM air quality in Korea: Background sources and related meteorological conditions

2013 년 8 월

서울대학교 대학원

지구환경과학부

이 승 민

The influence of trans-boundary air pollutants from neighboring countries on the PM air quality in Korea: Background sources and related meteorological conditions

By

Seungmin Lee

Dissertation Submitted to the Faculty of the Graduate School of the Seoul National University in Partial Fulfillment of the Requirement for the Degree of Doctor of Philosophy

Degree Awarded:
August 2013

Advisory committee:

Professor	Rokjin Park,	Chair
Professor	Chang-Hoi Ho,	Advisor
Professor	Jong-Ghap Jhun	
Doctor	Sang-Boom Ryoo	
Doctor	Lim-Seok Chang	
Professor	Yong-Sang Choi	

이학박사학위논문

주변 국가들로부터 이동해 오는 대기오염물질이 한국의 대기질에 미치는 영향 연구

The influence of trans-boundary air pollutants from neighboring countries on the PM air quality in Korea: Background sources and related meteorological conditions

2013 년 8 월

서울대학교 대학원

지구환경과학부

이 승 민

주변 국가들로부터 이동해 오는 대기오염물질이 한국의 대기질에 미치는 영향 연구

The influence of trans-boundary air pollutants from neighboring countries on the PM air quality in Korea: Background sources and related meteorological conditions

지도교수 허 창 회

이 논문을 이학박사 학위논문으로 제출함

2013년 4월

서울대학교 대학원

지구환경과학부

이 승 민

이승민의 이학박사 학위논문을 인준함

2013년 6월

위 원 장 _____ (인)

부위원장 _____ (인)

위 원 _____ (인)

위 원 _____ (인)

위 원 _____ (인)

위 원 _____ (인)

ABSTRACT

To improve air quality in Seoul, the city government has been bidding to curb emission of particulate matters in the past few years. However, the concentration of PM_{10} (particle matters with diameter < 10 ㎛) in Seoul is still high and frequently exceeds the daily environmental control standard of 100 μg m^{-3}. The present thesis examines the origin of and favorable meteorological conditions for high concentrations of PM_{10} in Seoul, Korea, in conjunction with systematic PM_{10} pathways.

First, high-PM_{10} episodes, defined as days in which the 24-h mean PM_{10} exceeds 100 μg m^{-3}, occurred 254 times during the period 2001–2008. Based on back trajectory and clustering analyses, the background sources of the high PM_{10} in Seoul are categorized as external (176 episodes) and internal sources (78 episodes). The primary external sources include the industrial areas in north eastern and central eastern China and the Gobi desert. The ratio of external to internal sources varies strongly according to the season, with highs in winter and spring and lows in summer. A composite analysis of meteorological factors for high-PM_{10} episodes with respect to the two sources (i.e., external and internal) suggests that an anomalous high pressure over Korea accompanied by an anomalous low pressure over the source regions favors both upper level transport

from the external source regions and the local accumulation of atmospheric PM_{10} in Seoul.

Next, the extraordinarily long-lasting episode of high concentrations of PM_{10} in Seoul, Korea over the period October 16–20, 2008 is closely examined. Satellite retrievals showed pronounced transport of aerosols from China to the Korean peninsula prior to the high-PM_{10} episode. The updraft of air pollutants from the source region in China, transport by westerlies, and subsequent descent to Seoul metropolitan regions are examined in the context of horizontal and vertical airflows. The connection between PM_{10} concentration over the Chinese source region and the Seoul target area is verified by wind back trajectory analysis. The meteorological conditions favorable for maintenance of the high PM_{10} levels are investigated through the analysis of weather maps and low-level stability. Air pollutant migration from China to Korea is verified by California Puff dispersion modeling.

Finally, extraordinarily long-lasting high-PM_{10} episodes in recent years are additionally examined. Commonly, the migratory anticyclone aroused by terrain characteristics in China causes the high-PM_{10} level in source regions. The air pollutants moves from source regions to Korea with the migratory anticyclone and induced westerly. Movement of pressure patterns and relevant wind flow changes may play crucial role in the transport of pollutant matters from source

regions to Korea.

Keywords: PM_{10}, Korea, China, Background source, Transboundary air pollutant, Meteorological condition

Student number: 2008-30821

TABLE OF CONTENTS

LIST OF FIGURES

LIST OF TABLES

1. INTRODUCTION

1.1. Background

In recent decades, remarkably rapid development of industry in China has resulted in economic growth, but also a large increase in energy consumption. The total energy consumption of China in the 2000s increased by about three times compared to the 1970s. A large increase in coal combustion has resulted in tremendous emissions, and these have become a major anthropogenic contribution to air pollution in China (He et al., 2002; Chan and Yao, 2008; Fang et al., 2009). Figure 1.1 shows the spatial distribution of aerosol over the East Asia region. AOD_{550} value is very high over the northeastern and central China. Considering there are many industrial sources, power plants, and large cities such as Beijing, Tianjin, Shenyang, and Shanghai in this area, the amount of air pollutants emitted from coal combustion and heavy traffic volumes could be very large. Hebei, Shandong, Jiangsu, Henan, Shanxi, and Sichuan provinces in this region are the largest contributors to PM_{10} emission in China (Zhang et al., 2009).

More troubling is the fact that the emission of particulate pollutants in China may cause severe air pollution problems not only in China, but also in

adjacent countries. Many previous studies reported that the air quality in Seoul, Korea is seriously affected by the influx of transboundary air pollutants emitted from large cities and industrial complexes in China, as Seoul is located downwind of China (e.g., Han et al., 2008; Koo et al., 2008, 2012; Kim et al., 2009; Heo et al., 2009; Lee et al., 2011).

Air pollution is known to be related to several social and economic issues, such as public health, traffic congestion from visibility reduction, mechanical failure in facilities, and deterioration of plant growth (Harrison and Yin, 2000; Hong et al., 2002; Al-Saadi et al., 2005; Pope III and Dockery, 2006; Lau et al., 2008; Hyslop, 2009). For this reason, air quality in Seoul is a major concern to the government and the general public. The concentration levels of air pollutants in Seoul are reported to citizens in real time through electronic quotation boards on the streets. Air quality forecasts are made on the news alongside weather conditions. In spite of the popular interest, Seoul, the capital and largest city in Korea, which has an exceptionally high population and high vehicle densities, frequently suffers from severe air pollution episodes (e.g., Kim et al., 2007; Lee et al., 2011).

Over the past few years, the Seoul city government has attempted to control and reduce locally emitted air pollutants through various schemes, such as supplying natural gas vehicles, replacing diesel buses with those powered by

liquefied petroleum gas, regulating pollutant emission from factories, and upgrading fuel quality (Kim and Shon, 2011). Thanks to these multilateral efforts, air quality in Seoul has steadily improved over the past few years. However, the concentration of particulate matter with a diameter <10 μm (PM_{10}) in Seoul is still higher than that in other large cities in advanced countries (Korean Ministry of Environment, 2007; Fig.1.2), and frequently exceeds the daily environmental control standard of 100 μg m^{-3}. This demonstrates that the reduction of local emissions is not sufficient to improve air quality in Seoul's metropolitan regions. To make more effective PM_{10} control strategy, it is important to estimate the main causes of high PM_{10} episodes: (i) the background source regions of PM_{10} and (ii) the meteorological factors influencing PM_{10} levels. Furthermore, the impacts of transboundary air pollutants from China, in addition to those locally emitted air pollutants, cannot be ignored in formulating a more effective PM_{10} control strategy.

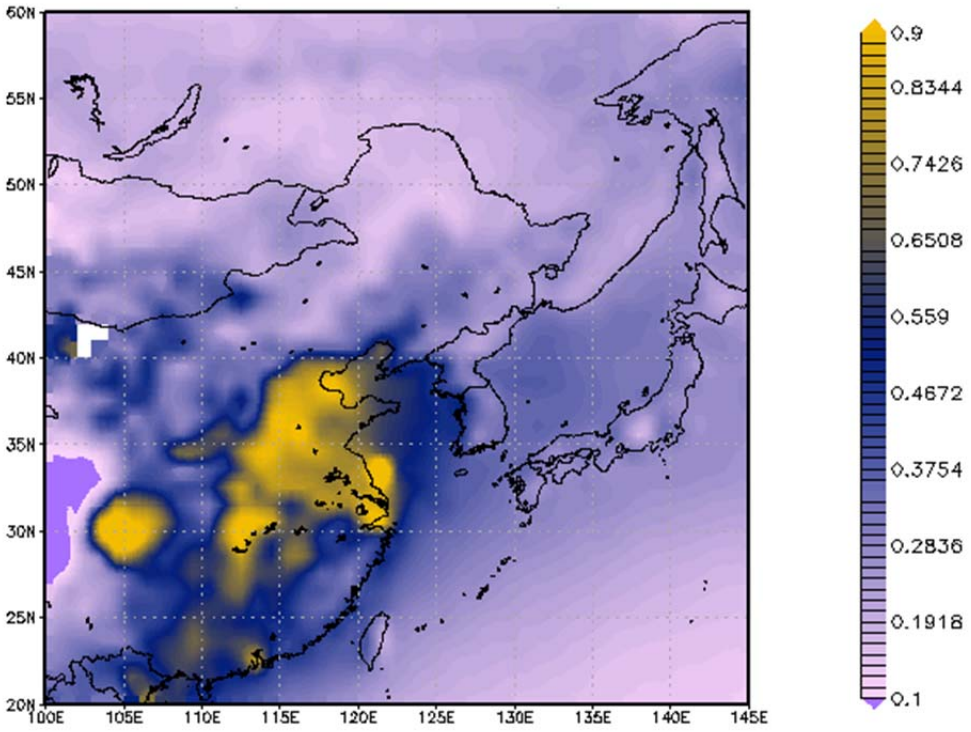

Fig. 1.1. Spatial distributions of the 12-year mean value of Terra-MODIS AOD_{550} from January 1, 2001 to December 31, 2012.

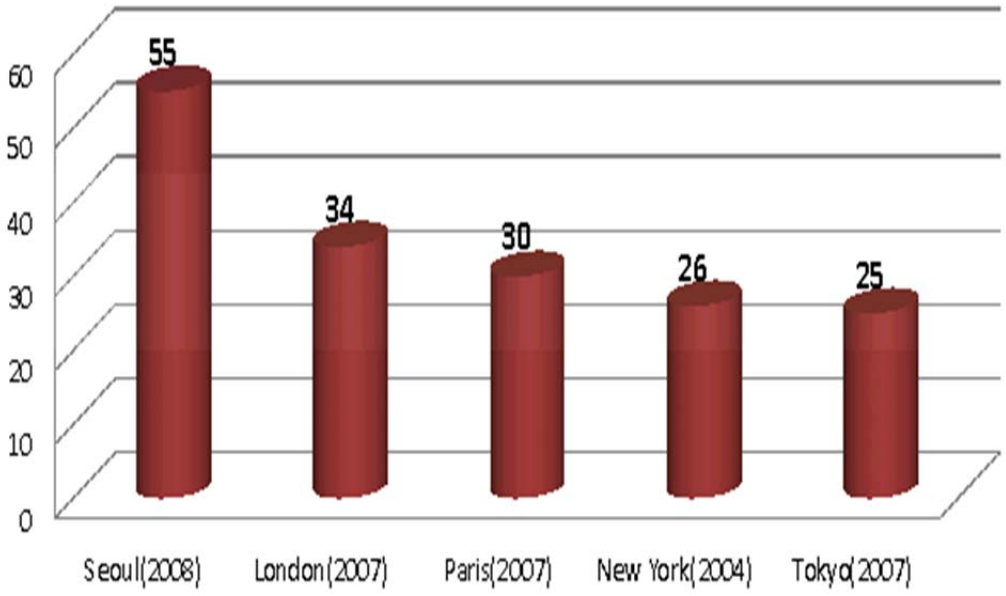

Fig. 1.2. The yearly mean concentration of PM_{10} (μg m^{-3}) in large cities of the world.

1.2. Objective of the thesis

First of all, we attempt to identify the background source regions of high PM_{10} in Seoul and quantify the contributions of those regions. The PM_{10} concentration level is modulated by local emissions from the usage of fossil fuel and the volume of traffic. It is also affected by the growing influx of transboundary particles from adjacent countries, as Seoul is located on the edge of the continent of Asia and lies in a belt of prevailing westerly (Kim et al., 2009). Regional control strategies for air pollutants in downwind countries might be ineffective without considering the effects of long-range transport of pollutants from external region. (Wuebbles et al., 2007). Several studies have revealed the influence of local emission sources (Kim et al., 1999; Kim and Kim, 2000; Park et al., 2004) and long-range transport of pollutants from external source regions on PM_{10} concentration in Seoul (Lee et al., 2001; Yi et al., 2001; Kim et al., 2007, 2009). However, most of those studies have focused only on one of many local and external sources or just on few cases during a short period. There exist only limited studies that deal synthetically with the contributions of various sources during a period long enough to characterize climatology of PM_{10} in Seoul. Here, we have classified the high PM_{10} episodes in Seoul into local and external source classes and quantified the contribution of

each class using back trajectory and clustering analysis methods.

Secondly, we attempt to clarify favorable meteorological conditions for high PM_{10} episodes using composite analyses of regional-scale meteorology in conjunction with the pathways of pollutants. Since some of air pollutants in Seoul are from external source regions, its transboundary transport, especially from China, should be accounted for. Many researches, however, focused on local meteorological data confined to the region of interest, and tried to reveal the influence on high PM_{10} episodes (Glen et al. 1996; Smith et al., 2001; Jiang et al. 2004). Such limited studies may not fully verify the origination, transport, and accumulation process of pollutants. In this study, we examine the meteorological condition over possible source regions and accumulation in Seoul from regional-scale composite analysis and confirmed the transport route from the pathway analysis. Furthermore, we have compared the meteorological condition between internal and external source types by the composite analysis and clarified impact of wind and pressure systems on the high PM_{10} episodes.

Thirdly, we attempt to closely investigate representative high-PM_{10} episode caused by trans-boundary air pollutants from China. In the period October 16-20, 2008, an extraordinarily long-lasting high-PM_{10} episode occurred in the Seoul area. This episode is significant because its seriousness is in stark contrast to the overall improvement of air quality in 2008. Focusing on this case, we attempt to

identify the processes responsible for the high-PM_{10} level occurrence, and its possible causal links with China-originated air pollutants. Here, we analyze several ground-based and remote sensing datasets to confirm the influence of trans-boundary air pollutants from China on the air quality in Seoul. We also investigate the meteorological conditions to identify the cause of the extraordinarily long continuity of high PM_{10} levels.

Finally, we attempt to verify the air pollutant migration pattern by atmospheric dispersion modeling. Back trajectory and observation data analyses have some uncertainty, because these analyses cannot show the relation between aerosol migration and air flow pattern simultaneously. Atmospheric dispersion modeling clearly shows the transportation pattern of particulate matters along the air flow, because it uses both aerosol and meteorological data. We verify the source regions and related meteorological fields throughout the modeling result.

The aims of this study can be summarized as follows:

- ✓ To identify the background source regions of high PM_{10} in Seoul and quantify the contributions of those regions.
- ✓ To clarify favorable meteorological conditions for high PM_{10} episodes using composite analyses of regional-scale meteorology in conjunction with the pathways of pollutants.

- ✓ To closely investigate representative high-PM_{10} episode caused by trans-boundary air pollutants from China using several observational datasets.
- ✓ To verify air pollutant migration from China to Korea by atmospheric diffusion modeling.

This dissertation is organized as follows.

Chapter 2 describes the research domain, monitoring data, and criteria of high-PM_{10} episode. The background source regions and relevant meteorological conditions of high PM_{10} in Seoul are investigated in Chapter 3. Possible mechanism of high-PM_{10} episode is described in Chapter 4 by close analysis of representative episodes in recent years. Finally, the summary and discussion is presented in Chapter 5.

2. DOMAIN AND DATA

2.1. Research domain

Seoul, the chosen region for the study (Fig. 2.1) is the capital of Korea and, as such, the center of its government, economy, and culture. Seoul has very high population density over 17,000 persons km^{-2} (Sung and Oh, 2011) and heavy traffic over 3 million vehicles (Korean National Statistical Office, 2006), which play a role for local emission of pollutants. Furthermore, Seoul is affected by air pollutants from external sources especially in China as it is close to large cities and industrial area in China and the Gobi desert, a major source for dusts, and the Yellow Sea, a source of sea salts (Lee et al. 2001; Kim et al. 2009). Industrial pollutants, dusts, and sea-salt particles from those regions may blow over Seoul on the prevailing westerlies.

Seoul frequently suffers from severe air pollution problem due to locally emitted and transported particulate matters from neighboring countries. Premature deaths and social costs from air pollution are estimated to be as high as one hundred thousand people and more than ten billion dollars every year (Gyeonggi Research Institute, 2003). Although the city government has been working to curb particulate matter emissions over the past few years, the

concentration of PM_{10} in Seoul is still two to three times higher than that in other large cities in Organization for Economic Cooperation and Development (OECD) countries (Korean Ministry of Environment, 2007).

2.2. Monitoring data

An eight-year hourly data series (2001–2008) of PM_{10} from 27 air quality monitoring stations in Seoul (Fig. 2.1) is examined. The stations are almost evenly distributed within the domain. To minimize the influence of the local effects of high fluctuations of PM_{10} (e.g., vehicles and industrial plants), only the monitoring stations that are located on isolated buildings in an open area were selected for analysis (Korean Ministry of Environment, 2008). Currently, PM_{10} is measured by the beta-ray absorption method, which utilizes the fact that part of the beta rays are absorbed and dissipated by the substance when the rays irradiate particulate matter collected on filter tape. This method has the advantage of affording real-time data with high temporal resolution (< 1 hour). However, we should also note that a < 10% measurement error can be caused by the inflow of particle-containing moisture (Chang and Tsai, 2003; Jung et al., 2007).

Meteorological data for the same period as PM_{10}, including zonal, meridional, and vertical wind (u, v, and w), as well as air temperature, relative humidity, and geopotential height, are obtained from the National Centers for Environmental Prediction-National Center for Atmospheric Research (NCEP-NCAR) reanalysis (Kalnay et al. 1996) with a longitude-latitude resolution of 2.5° × 2.5°. Precipitation data are obtained from the Global Precipitation Climatology

Project's (GPCP) gridded 1° × 1° product (Huffman et al. 2001). Because of the influence of regional-scale meteorology on the occurrence of high-PM_{10} episodes, we use globally observed meteorological data in conjunction with locally observed PM_{10} data. Because high-PM_{10} episodes occurred in all seasons, we use anomalies against daily climatology for meteorological data to identify the meteorological characteristics of high PM_{10} concentration, excluding seasonality.

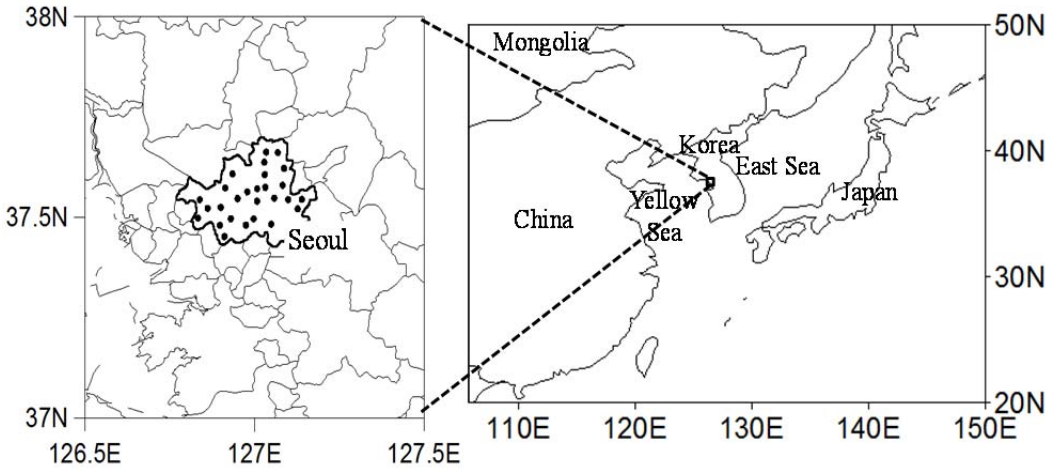

Fig. 2.1. Monitoring sites of PM_{10} in Seoul, Korea.

2.3. High PM_{10} episodes in Seoul

In order to identify the high-PM_{10} days in Seoul, the daily as well as the spatial-mean values of hourly surface PM_{10} data are examined. On the basis of the standard value specified in the current environmental protection law (a daily-mean value of 100 $\mu g\ m^{-3}$), days with $PM_{10} > 100\ \mu g\ m^{-3}$ are defined as high-PM_{10} episodes. 100 $\mu g\ m^{-3}$ is also the standard value for issuing and lifting of air pollution alerts in Seoul. It is necessary to distinguish high-PM_{10} episodes from yellow dust episodes. Both cause high PM_{10} concentrations, but the yellow dust episodes are harder to control because they occur as a result of natural sources. Several previous studies (Shin et al., 2007; Koo et al., 2010) have dealt with high-PM_{10} episodes as distinguished from yellow dust episodes. Among the 346 days of high-PM_{10} episodes for the analysis period, 92 days of yellow dust are excluded from the analysis (Fig. 2.2). In the figure, the days of high PM_{10} without a mark (●) are interpreted as yellow dust episodes. Finally, a total of 254 days are selected as the high-PM_{10} episodes (Table 2.1). As mentioned in the previous section, high-PM_{10} episodes, which occur in all seasons, are different from yellow dust episodes, which mainly occur in spring (Fig. 2.2). As seen in Table 2.1, the number of high-PM_{10} days and the yearly mean concentration of PM_{10} have been gradually declining since 2001. However, the PM_{10} level in

2008 (55.66 μg m^{-3}, the lowest level for 2001–2008) still exceeds the environmental standard (50 μg m^{-3} as the annual mean).

We also define low-PM_{10} episodes as the days when the PM_{10} levels are less than 25 μg m^{-3} (Fig. 2.2). Unlike the high-level of PM_{10} episodes, there is no legal standard value to define low concentration episodes. The threshold value of 25 μg m^{-3} for low-PM_{10} episodes has been selected in such a way that the number of low PM_{10} episodes is similar to the number of high-PM_{10} episodes. A total of 272 days are selected as low-PM_{10} episodes (Table 2.1). The low-PM_{10} episodes mostly occurred in summer. Over the past three years, the number of low-PM_{10} days has conspicuously increased.

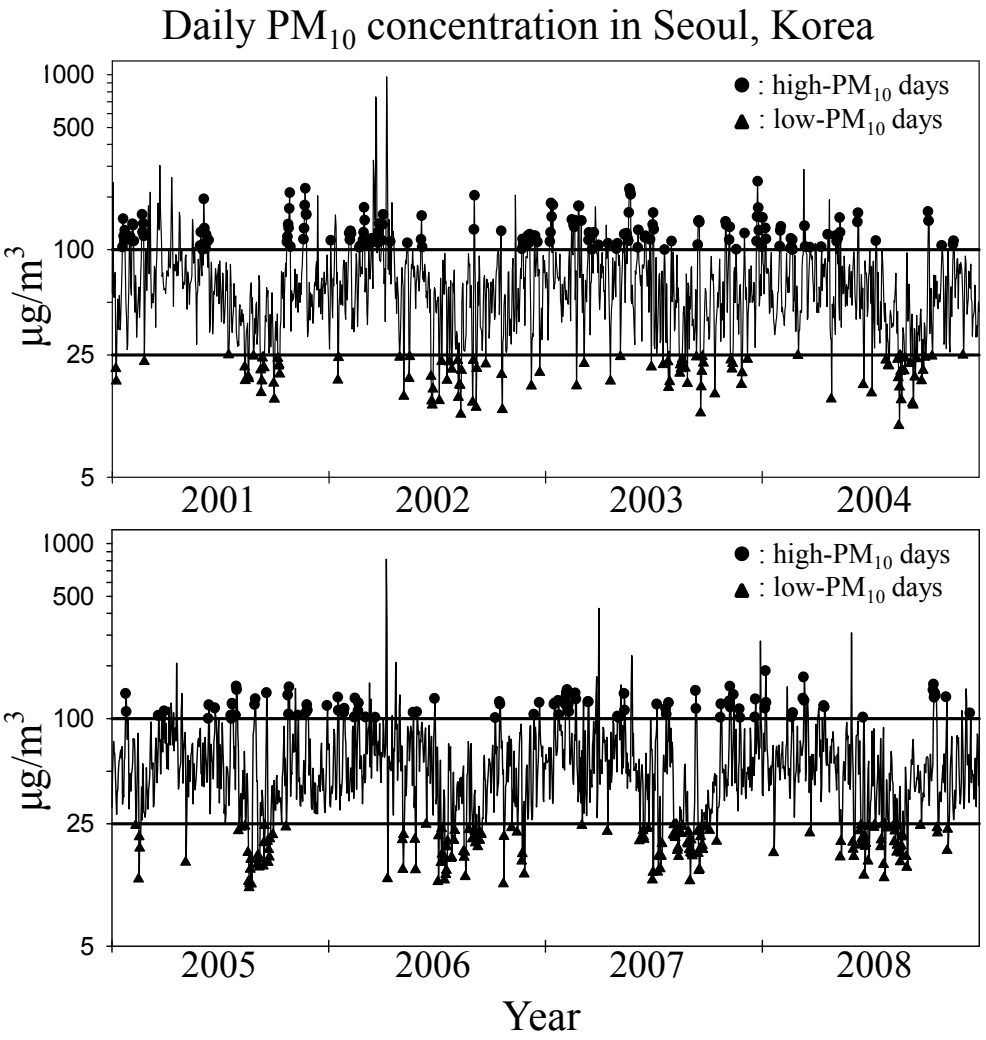

Fig. 2.2. The time series of daily PM_{10} concentration observed in Seoul, Korea. Upper and lower thick horizontal lines indicate reference values of high- and low-PM_{10} episode, respectively. Closed circles and triangles indicate high- and low-PM_{10} episodes, respectively.

Table 2.1. Number of high and low PM_{10} days and yearly-mean concentration of PM_{10} for each year during the period from 2001 to 2008.

Year	Number of high-PM_{10} days	Number of low-PM_{10} days	Annual-mean PM_{10} concentration ($\mu g\ m^{-3}$)
2001	38	20	69.90
2002	35	30	74.73
2003	55	29	69.30
2004	29	27	60.65
2005	26	29	57.35
2006	18	44	58.85
2007	35	48	60.84
2008	18	45	55.66
Total	**254**	**272**	**63.41**

3. BACKGROUND SOURCES AND RELEVANT METEOROLOGICAL CONDITIONS FOR HIGH PM_{10} EPISODES IN SEOUL

3.1. Identification of background sources by back trajectory analysis

Because of its usefulness in identifying transboundary sources, the wind back trajectory analysis method is commonly used in many air pollution researches (Stohl, 1996, 1998; Niemi et al., 2004; Borge et al., 2007; Ariano et al., 2008; Vardoulakis and Kassomenos, 2008; Kim et al., 2009). Back trajectory analysis provides a better understanding of the air flow and transport patterns of air pollutants. Generally, the confidence in cluster analysis on the back trajectories increases with the number of trajectories analyzed (Borge et al., 2007). For these reasons, back trajectories for the 254 cases during relatively long periods (2001–2008) are analyzed in the present study (Fig. 3.1), whereas most of the previous studies used short-term monitoring data or analyzed a limited number of specific episodes.

We calculate the back trajectories of each high-PM_{10} episode using the FLEXTRA trajectory model (Stohl et al., 1995; Stohl and Seibert, 1998).

Temperature, 3-dimensional wind, specific humidity, and surface pressure are used as the input data for plotting 72-hour back trajectories. Researchers use 72-hour back trajectories to identify air mass pathways while considering the transport time of air pollutants (Hwang and Ro, 2005; Lee et al., 2008; Kim et al., 2009). The arrival point at 00 UTC on the day of a high-PM_{10} episode is Songwol-dong, Jongno-gu, Seoul (37.57°N, 126.97°E). Considering boundary layer, 1,000 m above the surface is settled as arrival height. The time interval between trajectory points is three hours. The trajectory type is 3-dimensional, and all three wind components are used.

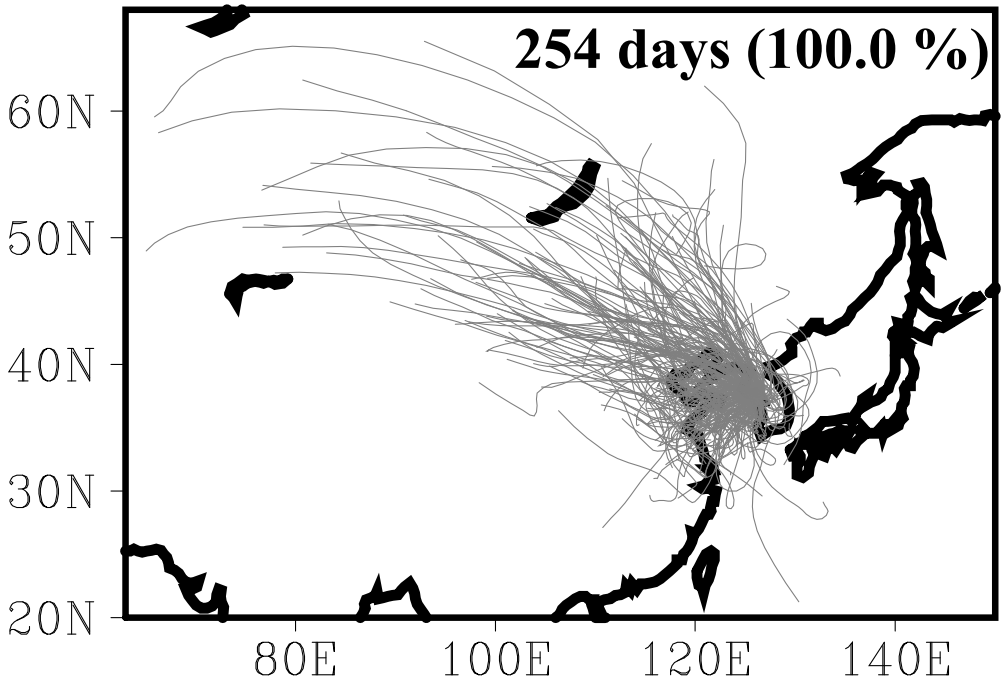

Fig. 3.1. Back trajectories of all high- PM_{10} concentration days.

3.2. Classification of high PM_{10} episodes by clustering analysis

It has been demonstrated that the clusters of back trajectories arriving at a specific location can effectively classify different synoptic circulation patterns (Dorling et al., 1992; Dorling and Davies, 1995; Borge et al., 2007). In this study, an agglomerative hierarchical clustering algorithm based on the Euclidean distance measure and the Ward's minimum variance clustering criterion is applied to the back trajectories using MATLAB. The longitudes and latitudes of the trajectories over 3-hour intervals are used as clustering variables. The number of clusters is determined by assessing where noticeable increases in the distances between merged clusters occur (Fig. 3.2).

To classify the source regions of high PM_{10} levels, we categorize the back trajectories of the 254 high-PM_{10} episodes into three groups via clustering analysis (Fig. 3.3). The trajectories belonging to the first group (Fig. 3.3a) are short and are confined around the Korean peninsula and the Yellow Sea. This group accounts for 30.7% of the total (78 days among the 254 days). We suspect that the episodes in the first group are affected by local emissions, such as the use of fossil fuel, the volume of motor traffic, urban dust, and sea salt particles. The second group (Fig. 3.3b) accounts for the largest proportion (41.3% = 105 days among the 254 days). The trajectories belonging to this group broadly

extend over central and northeastern China, including a number of industrial regions, such as the northern industrial district (comprising major cities such as Beijing and Tianjin) and the northeastern industrial district (specializing in heavy chemical industry). We estimate that the episodes belonging to the second group resulted from transboundary air pollutants originating in many of the industrial facilities in China. Finally, the trajectories of the last group are extremely long, mostly stretching over the Gobi desert in Mongolia and even far central Asia (Fig. 3.3c). These kinds of episodes may occur from the long-range transport (LRT) of sand dust originating from the desert. The 71 days in the last group account for 28.0% of the total proportion. If we think of yellow dust episodes (92 days) as members of this group, the percentage of this group become much higher than other two groups.

For convenience, we name each group domestic-source type, northeastern China-source type, and desert-source type, in order. If we regard the northeastern China- and desert-source types as external-source types, a nearly two-thirds majority (176 days) of the total high-PM_{10} episodes are found to be caused by external sources, whereas only a third (78 days) of the total episodes are caused by local sources. The mean concentration of PM_{10} is 128.0 μg m^{-3} for the domestic-source type, 126.3 μg m^{-3} for the northeastern China-source type, and 127.6 μg m^{-3} for the desert-source type. Although these values are similar, if we

include yellow dust episodes in the desert-source type, it is most likely that the amount of PM_{10} in the desert-source type is by far the largest of all, having a mean value of 163.7 $\mu g\ m^{-3}$.

It should be noted that there is a limitation in identifying the pathways of air parcels using the back trajectory analysis, because emissions and depositions of air pollutants along the trajectories are not considered. Thus, calculated trajectories only approximately correspond to the mean transport routes of air pollutants. This limitation would be most serious for the external source types (i.e., desert-source and northeastern China-source), whose proportion may be overestimated. Nevertheless, our results clearly indicate that the air pollutants from outside contribute substantially to the occurrence of high-PM_{10} episodes in Seoul. To support this point, we analyze the PM_{10} records in Beijing and Tianjin in northern China during the periods from +2 to −7 day of high-PM_{10} episodes in Seoul for external source types (Fig. 3.4). Air pollution index data of the two cities are used for analysis. Fig.3.4 shows that the PM_{10} concentrations in the two cities increase rapidly from −3 day and reach its peak at −1 day. This supports the link between high PM_{10} events in external source regions and Seoul.

Fig. 3.5a shows the number of high-PM_{10} days for pathway types with respect to seasons. There are significant differences in the frequency of high-PM_{10} days among seasons. The most and least frequent episodes occur in

December–February (DJF, 92 days among 254 days) and June–August (JJA, 43 days among 254 days), respectively. The frequencies in March–May (MAM) and September–November (SON) are similar (59 and 60 days among 254 days, respectively). The seasonality for source types was investigated. In DJF and MAM, the frequency of external-source types (desert-source and northeastern China-source) is much higher (78 days in DJF and 46 days in MAM) than that of the local type (14 days in DJF and 13 days in MAM), whereas the local type occurs more frequently than the desert-source type in JJA. If we include the yellow dust episodes that mostly occur in spring, the predominance of the external type in the cold seasons is strengthened. In SON, the external type is a little more (36 days) than the local type (24 days). Summing up, the high-PM_{10} episodes caused by external sources occur more often than those caused by local types in all seasons except summer.

Fig. 3.5b shows the number of high-PM_{10} days for types with respect to years. We confirm the noticeable frequencies in 2003, which indicate the influence of large amounts of aerosols emitted by Russian forest fires during the period from April to August 2003 (Edwards et al., 2004; Damoah et al., 2004; Nedelec et al., 2005). Except for 2007, the downward trend of occurrence from local sources is distinct, which likely results from efforts by the city government to reduce pollutant emissions. In contrast, the decrease in frequencies from

external sources is unclear.

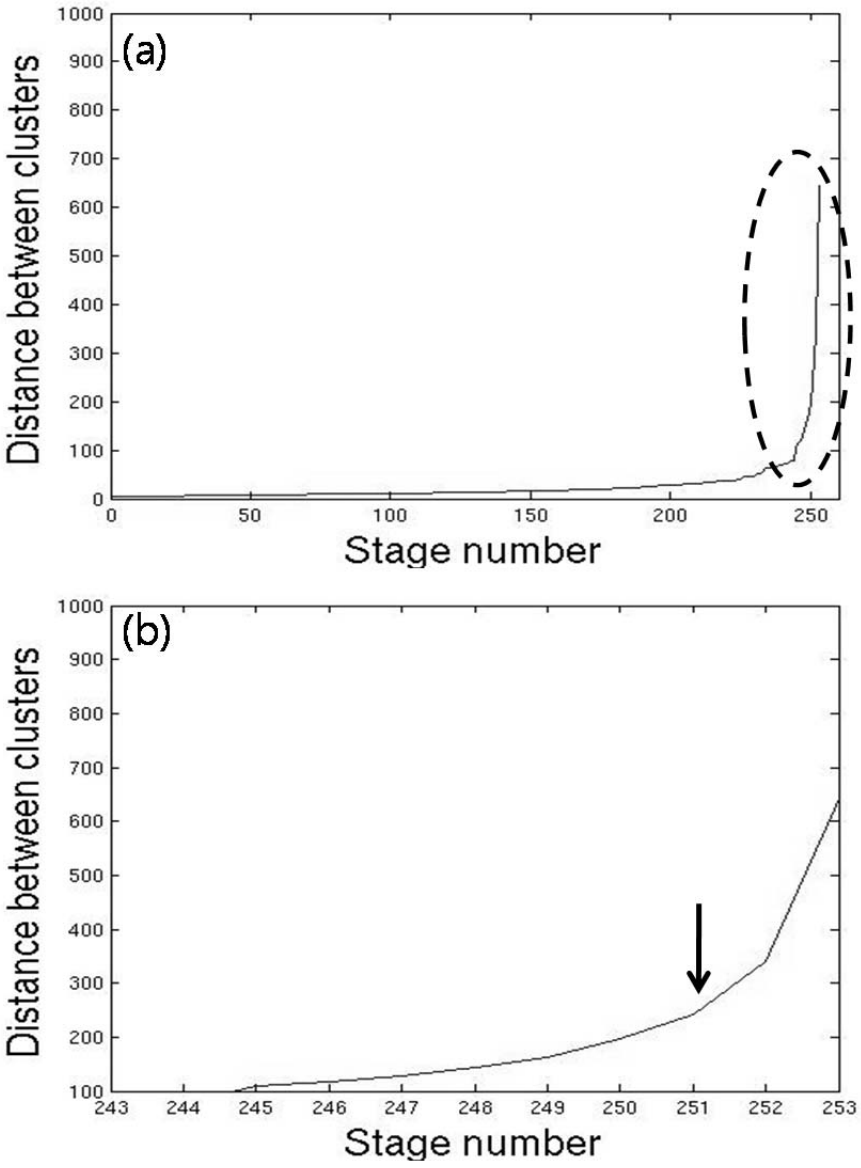

Fig. 3.2. Distance between merged clusters as a function of the stage of the cluster analysis for all high-PM_{10} episodes, for (a) all stages and (b) last ten stages. Arrow in (b) indicates the stage decided for the number of clusters.

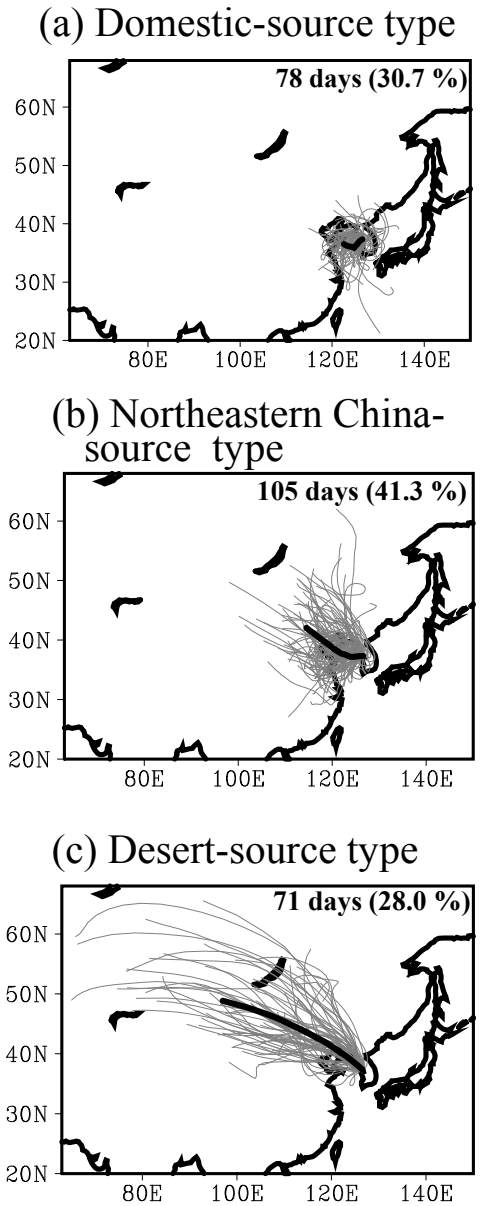

Fig. 3.3. Same as Fig. 3.1 except for (a) domestic-source type, (b) northeastern China-source type, and (c) desert-source type of back trajectories in high-PM_{10} concentration days. The thick lines indicate the average of trajectories. The numbers in each map are days and proportions.

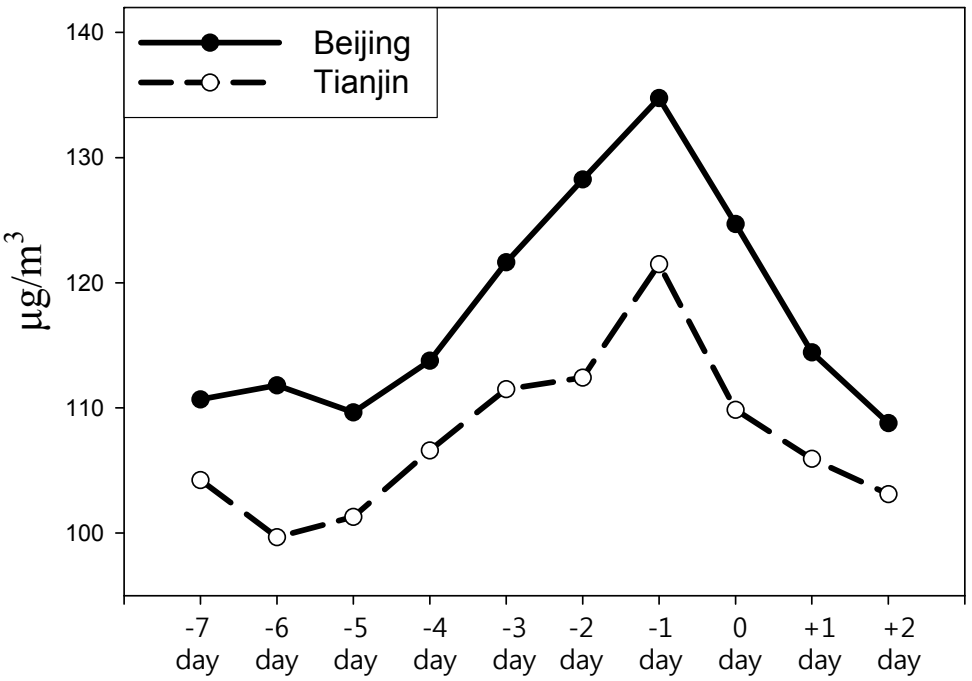

Fig. 3.4. The daily-mean PM_{10} concentrations observed in Beijing and Tianjin, China for the period from +2 to –7 day of high- PM_{10} episodes in Seoul for external source type.

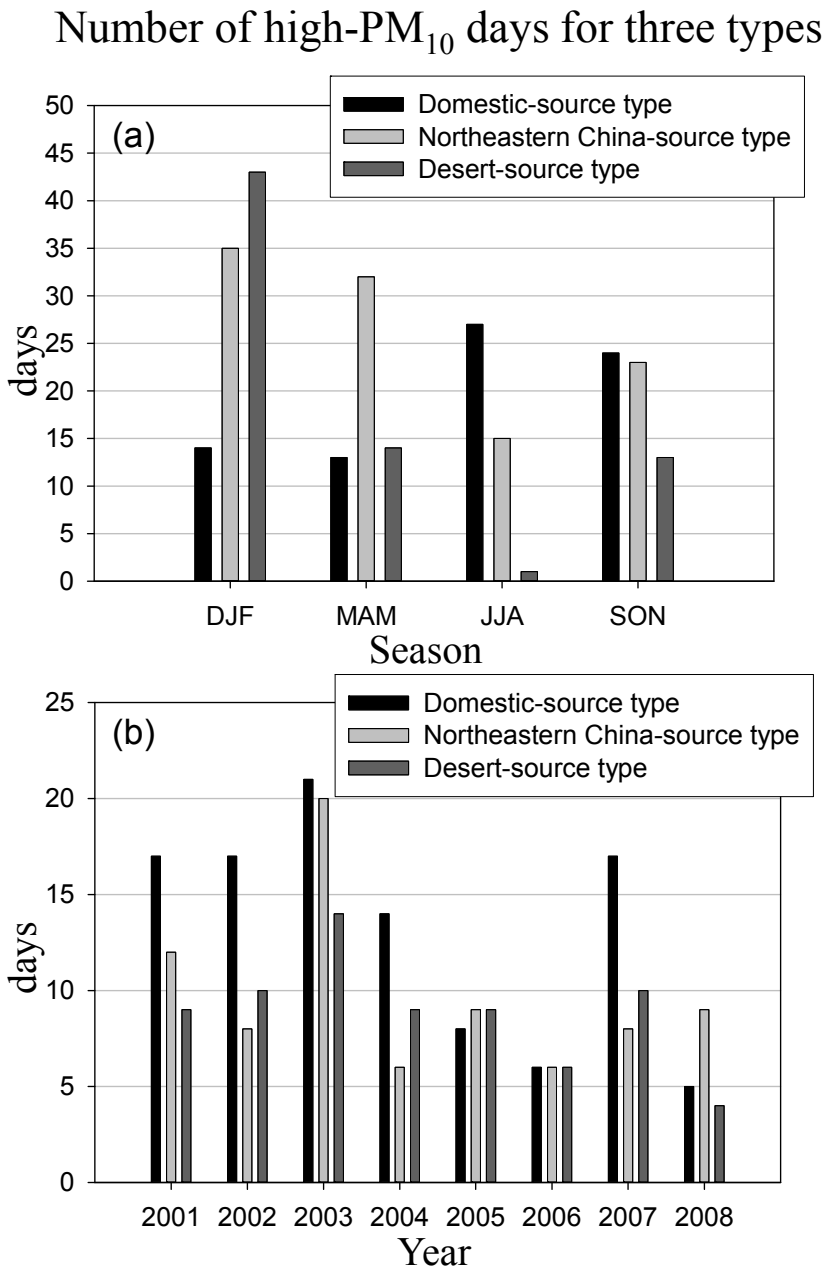

Fig. 3.5. The number of high-PM_{10} days for three types (domestic-source, northeastern China-source, and desert-source types) in (a) each season and (b) each year.

3.3. Relation between PM_{10} concentration and local meteorological factors in Seoul

To investigate the influence of meteorological factors on PM_{10} concentration, relation between PM_{10} concentration and locally observed meteorological data, such as wind direction, wind speed, rainfall, relative humidity. Used meteorological data are obtained from automatic weather system (AWS) located at Songwol-dong, Jongno-gu, Seoul (37.57°N, 126.97°E).

Firstly, we have analyzed the relation between PM_{10} concentration and local wind. Fig. 3.6a and b show the relation between the PM_{10} concentration and the local wind for the days except for yellow dust episodes (in 2008, mostly similar pattern in 2001–2007, figure not shown) and the days of yellow dust episodes (in 2001–2008), respectively. The PM_{10} concentration is high when the local wind is from the west (WNW, W, WSW, SW, and NW) for both the high PM_{10} episodes and yellow dust episodes. However, there are some distinctions between high PM_{10} episodes and yellow dust episodes. PM_{10} concentration is much higher in yellow dust episodes (up to 975.5 μg m^{-3}) than in high PM_{10} episodes (up to 246.2 μg m^{-3}). Wind speed is high in yellow dust episodes (mean value is 3.1 m s^{-1}), compared to low wind speed in high PM_{10} episodes (mean value is 1.8 m

s^{-1}).

Through the dominant westerly in high PM_{10} episodes, we can guess that high PM_{10} concentration in Seoul is due to transported air pollutants that emitted on the Western side of Korea (China and Mongolia). However, we should notice that the main wind in Seoul is westerly regardless of PM_{10} concentration, because Seoul is located in the belt of westerlies. Considering this, we calculated the mean value of wind speed for each wind direction from 2001 to 2008 (Fig. 3.7a). The level of PM_{10} concentration is high for the local wind from the west in every year. When the local wind is northeasterly, PM_{10} concentration is also high. Besides, from the decrease of inner area of polygon, we can guess the decrease of PM_{10} concentration in recent years. As mentioned in previous chapter, the yearly mean concentration of PM_{10} have been on the gradual decline since 2001, and the PM_{10} level in 2008 is 55.66 μg m^{-3}, which is lowest value since records began. To gain more detailed information about relation between PM_{10} concentration and wind speed, we have created box plot of PM_{10} concentration for each class of wind speed, for the days except for yellow dust episodes (Fig. 3.7b). Negative relationship between PM_{10} concentration and wind speed is confirmed again by the figure.

Next, we have analyzed the relation between PM_{10} concentration and rainfall and relative humidity. When it rains, PM_{10} concentration is low due to

scavenging effect of rainfall. We can check the negative relation between PM_{10} concentration and rainfall by Fig. 3.8a. Especially, the high PM_{10} episodes do not occur when the rainfall amount exceeds 20 mm. Fig. 3.8b shows the relation between PM_{10} concentration and relative humidity. The positive relationship of them is verified from the figure. It may be caused by attachment of moisture to particulate matters, which is in accord with preceding study of Shin et al. (2006). The occurrence of haze and smog may be associated with this positive relationship between PM_{10} concentration and relative humidity. Further details about this will be examined in my next step of Ph. D. degree course.

(a) PM_{10} vs Wind
(2008, except for Yellow dust episodes)

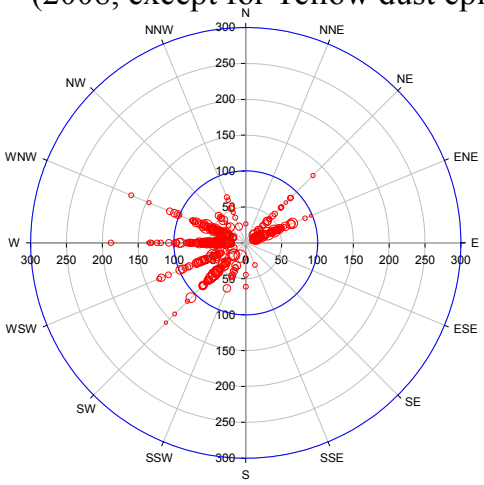

(b) PM_{10} vs Wind
(2001-2008, Yellow dust episodes)

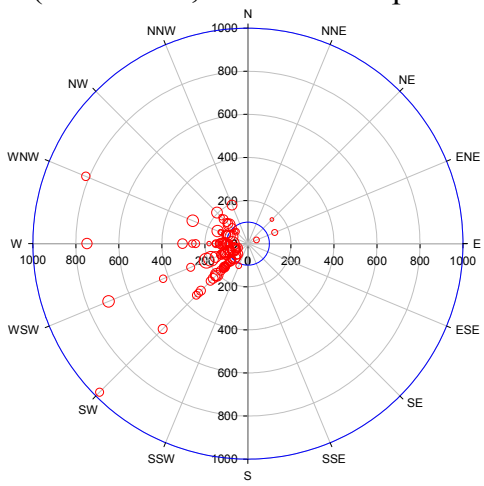

Fig. 3.6. The polar scatter plots of PM_{10}, leading wind direction and daily mean wind speed of Seoul (a) for the days in 2008 except for yellow dust episodes and (b) for the days yellow dust episodes in 2001-2008. The size of open circle indicates the wind speed, and the inner blue circles indicate the 100 $\mu g/m^3$ of PM_{10} concentration.

(a) PM_{10} vs Wind direction

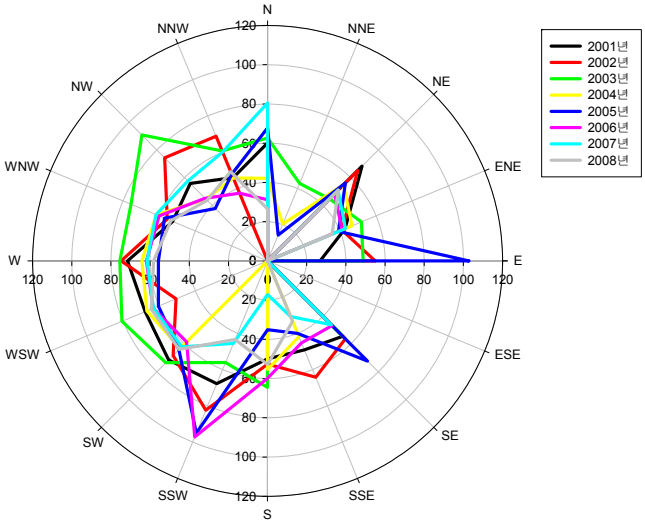

(b) PM_{10} vs Wind speed

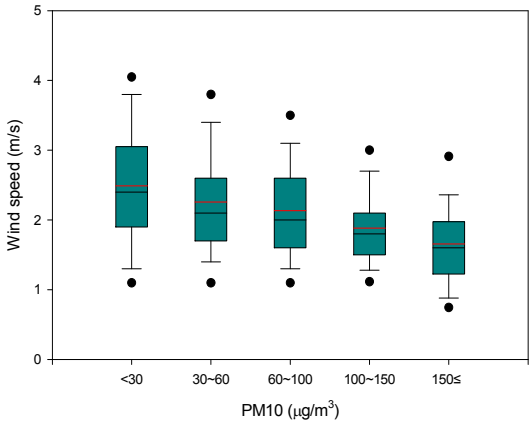

Fig. 3.7. (a) The polar line plots of PM_{10} and leading wind direction of Seoul from 2001 to 2008 except for yellow dust episodes. (b) The box plot of PM_{10} and daily mean wind speed of Seoul in the same periods of (a).

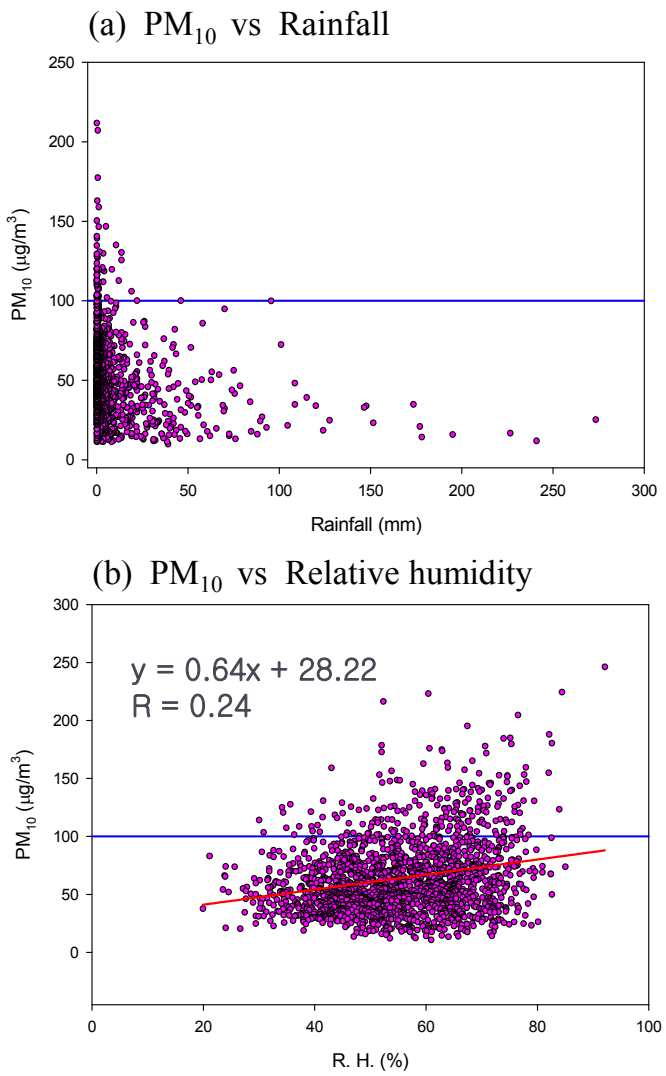

Fig. 3.8. (a) The scatter plot of PM_{10} concentration and rainfall amount for rainy days in 2001-2008 except for yellow dust episodes. (b) The scatter plot of PM_{10} concentration and relative humidity for the days in 2001-2008 except for dust episodes and rainy days. Blue horizontal line indicate the 100 $\mu g/m^3$ of PM_{10} concentration.

3.4. General features of the regional-scale meteorologies in high PM_{10} episodes

To identify the meteorological factors influencing high PM_{10} levels, we analyzed a composite of daily anomalies of meteorological factors for the high- and low-PM_{10} episodes (Fig. 3.9). Anomalously high temperatures and pressures occurred over the Korean peninsula during high-PM_{10} episodes, whereas the pattern for low-PM_{10} episodes is contrary to that for high-PM_{10} episodes (Figs. 3.9a, 3.9b, 3.9c, and 3.9d). The atmosphere is stable in the rear of the stationary high pressure, which is a good condition for the accumulation of pollutants. Higher temperatures may be related to greater local aerosol formation because of higher rates of chemical reactions (Van Der Wal and Janssen, 2000), contributing to higher PM_{10} concentration levels. Furthermore, during high-PM_{10} episodes, the lower troposphere is drier, which is a better condition for suspended particulates (Fig. 3.9e). Finally, the lower- and upper tropospheric winds are weaker over the Korean peninsula and neighboring regions in northeastern China during high-PM_{10} episodes (Figs. 3.9g and 3.9i). Weak winds not only prevent the dispersion air pollutants but also allow the accumulation of particulate matter in the system, whereas strong winds flush pollutants out of the system (Chaloulakou et al., 2003).

In contrast, there is a stronger positive rainfall anomaly around the Korean peninsula during low-PM_{10} episodes (Fig. 3.9f), so that the scavenging effect of rainfall significantly reduces PM_{10} concentration (Loosmore and Cederwall, 2004; Choi et al., 2008). For this reason, low-PM_{10} episodes mostly occurred in the rainy summer season (see Fig. 2.2).

The characteristics of meteorological fields are closely linked to the origination, transport, and diffusion of pollutants, as well as the formation of favorable conditions for the accumulation and dissipation of pollutants. Therefore, it is necessary to estimate the contribution of local and external influences on high PM_{10} levels through tracing the pathways of particulate matter. We will discuss these details in the next section.

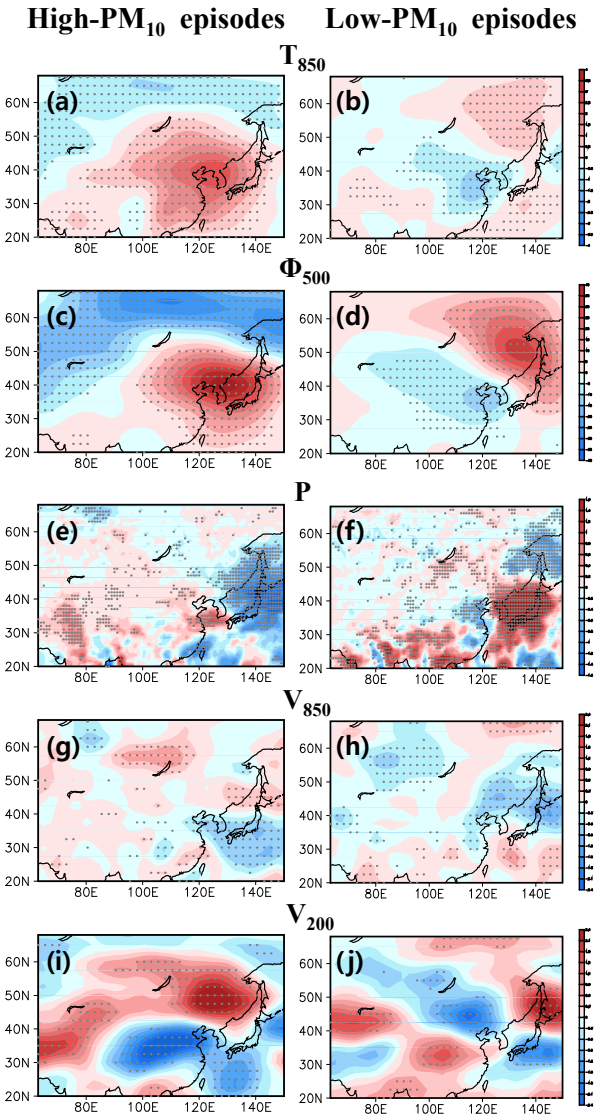

Fig. 3.9. Composite of anomalous 850 hPa air temperature (T_{850}, (a) and (b)); 500 hPa geopotential height (Φ_{500}, (c) and (d)); precipitation (P, (e) and (f)); 850 hPa wind speed (V_{850}, (g) and (h)); and 200 hPa wind speed (V_{200}, (i) and (j)). The left and right panels are cases of high- and low-PM_{10} episodes, respectively. Dots indicate grids with the 95% statistical significance based on a t-test.

3.5. Relation between the meteorological fields and the source type of high PM_{10} episodes

The meteorological fields affecting the high PM_{10} levels are closely connected with the pathways of PM_{10}. Therefore, we perform a composite analysis of meteorological factors for each pathway type to examine the differences among the three types. The results from this analysis show that the pressure, upper-level wind, and vertical wind fields are clearly distinguishable among the three types (Figs. 3.10 and 3.11), whereas the patterns of the other factors, such as precipitation, lower-level wind, temperature and relative humidity, are not distinct (figure not shown).

In the case of the local type, the upper wind speeds are weak, showing a pattern similar to the general features of high-PM_{10} episodes (Fig. 3.10a). The anomalous high located over the northern region of the Korean peninsula induces an anomalous easterly, weakening the westerlies over the central and southern regions of Korea (including Seoul). As a result, the wind in Seoul is calm, which is a favorable condition for the accumulation of locally emitted particulate matter. In the case of the northeastern China-source type, the anomalous high is located somewhat to the east of the local type, and the anomalous low is located over

Kazakhstan, inducing an anomalous upper westerly over the Taklimakan desert (Fig. 3.10b).

The meteorological field for the desert-source type is fairly different from the above two types. The desert-source type occurs when the upper tropospheric wind is strong (however, the lower wind is weak and likely contributes to the accumulation of pollutants) (Fig. 3.10c), which is slightly different from the general features of high-PM_{10} episodes. It is apparent that strong anomalous westerlies at 200 hPa occur along the pathways of the pollutants. The southward-shifted anomalous high compared with the local type induces the upper westerly over the central and northern regions, intensifying the upper westerlies in Seoul. In addition, an anomalous low over northern Mongolia is likely to induce ascending motions and to intensify the upper-level westerly over the Gobi desert, supplying and transporting dusts eastward (this is confirmed in Fig. 3.11). In the case of the desert-source type, the ascending motions are located over the Gobi and Taklimakan deserts from two days prior, supplying dust to the upper troposphere (Figs. 3.11a and 3.11b). Also, a descending motion over Seoul on the high-PM_{10} days assists the fallout of the transported dusts (Fig. 3.11c). Our findings are supported by previous studies showing that pollutants arising from source regions are transported in the upper atmosphere for long distances over a few days via jet streams (Huang et al. 2008; Sun et al. 2001). Unlike the desert-

source types, significant values of vertical wind anomalies are not located over the external source regions in the local and the northeastern China-source types (figure not shown).

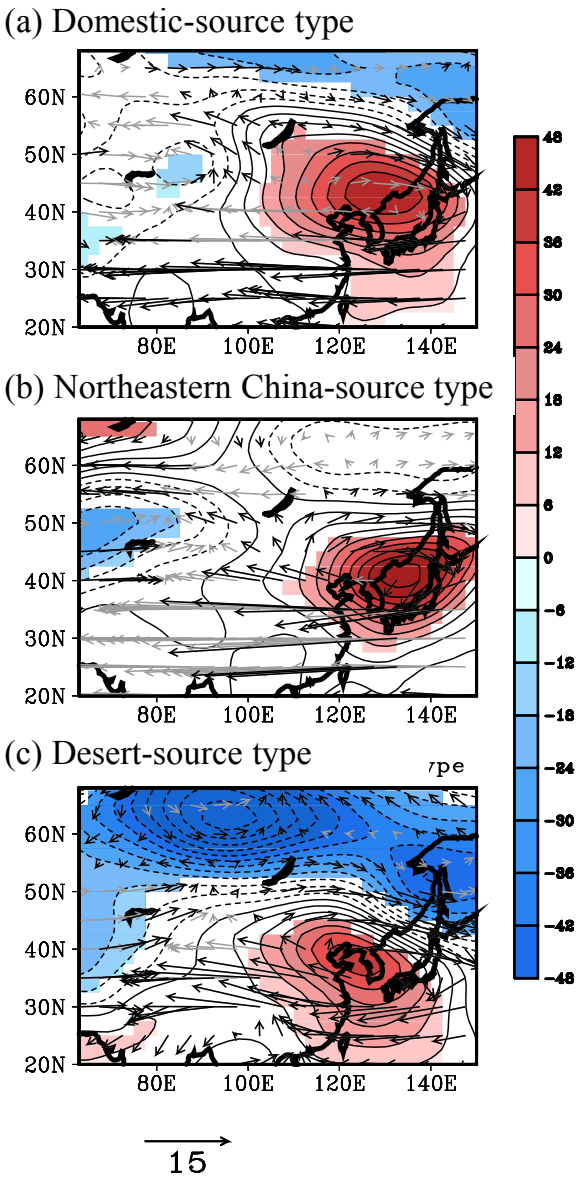

Fig. 3.10. Composite analysis in anomalous 500 hPa geopotential height (contour) and 200 hPa wind vector (arrows) for (a) domestic-source type, (b) northeastern-source type, and (c) desert-source type. Shading and dark arrows denote regions significant at the 95% confidence level based on a t-test.

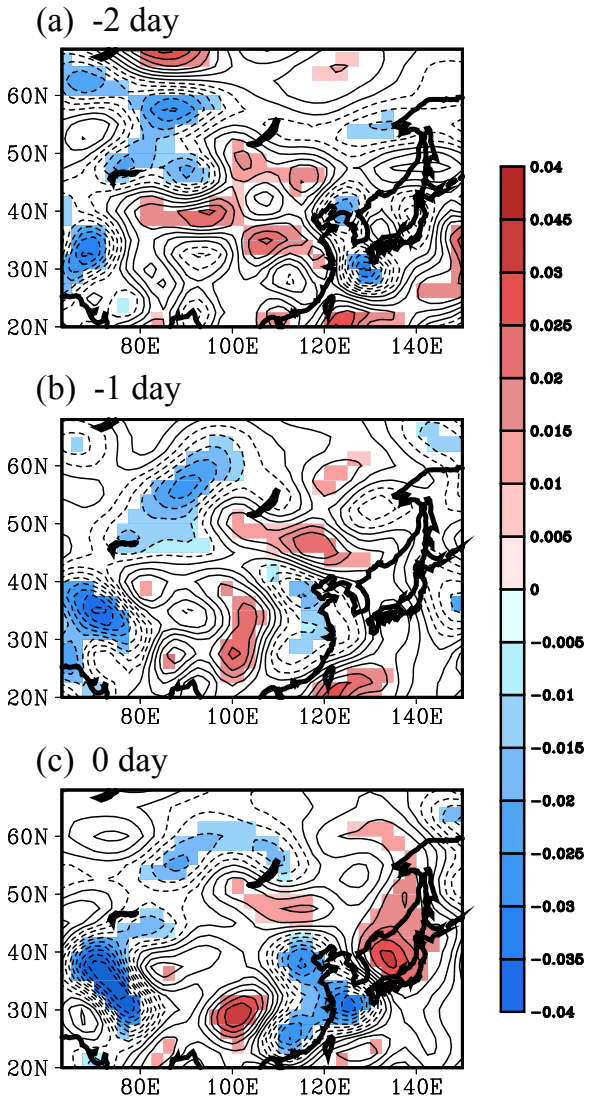

Fig. 3.11. Composite analysis in anomalous 850 hPa vertical wind (contour) for (a) two days before, (b) the previous day, and (c) the high-PM_{10} day. Shading denotes the regions significant at the 95% confidence level, based on a t-test.

4. CASE STUDY

4.1. A case of high PM_{10} episode during October 16-20, 2008

As mentioned in the introduction, air quality in Seoul has significantly improved through multilateral efforts to reduce local emissions of air pollutants. Consequently, the concentration of PM_{10} in 2008 reached a minimum during the study period (from 2001 to 2008). The level of PM_{10} in 2008 was 55.7 μg m^{-3}, falling by 20% from 69.9 μg m^{-3} in 2001. The high-PM_{10} episode in October 2008, ironically, lasted about a week, which is a historical record long in recent decades. We focus on this episode and closely investigate the cause of its extraordinarily long continuity against an overall improvement of air quality.

The levels of PM_{10} concentration, averaged over 27 air quality monitoring stations in Seoul (Korean Ministry of Environment, 2008), are displayed for the period October 11–25, 2008 (Fig. 4.1). From 14:00 on October 15, the PM_{10} concentration begins to increase above the environmental control standard value (100 μg m^{-3}), and reaches the first peak, 181.0 μg m^{-3} at 20:00 on October 16. Following this, it shows a slight decreasing tendency, but still remains above 100 μg m^{-3}. From the afternoon of October 19, the PM_{10} concentration increases

again up to 197.2 μg m^{-3} at 20:00, attaining its maximum value. A drop of PM_{10} level below 100 μg m^{-3} only occurs after 05:00 on October 21. The five day-mean PM_{10} concentration during the high-PM_{10} episode is 142.3 μg m^{-3}, which is 80–100 μg m^{-3} higher than the background 58.7 μg m^{-3} before and 44.4 μg m^{-3} after the episode. During the high-PM_{10} episode, haze was observed all over Seoul, which may be caused by the large concentrations of pollutants in the air. As seen in lower panels of Fig. 4.1, before and during the high-PM_{10} episode, westerly winds prevailed. When the wind hauls around to the east-northeast on October 21, PM_{10} concentration levels begin to decrease. It drops sharply below 50 μg m^{-3} after rain events on October 22 and 23.

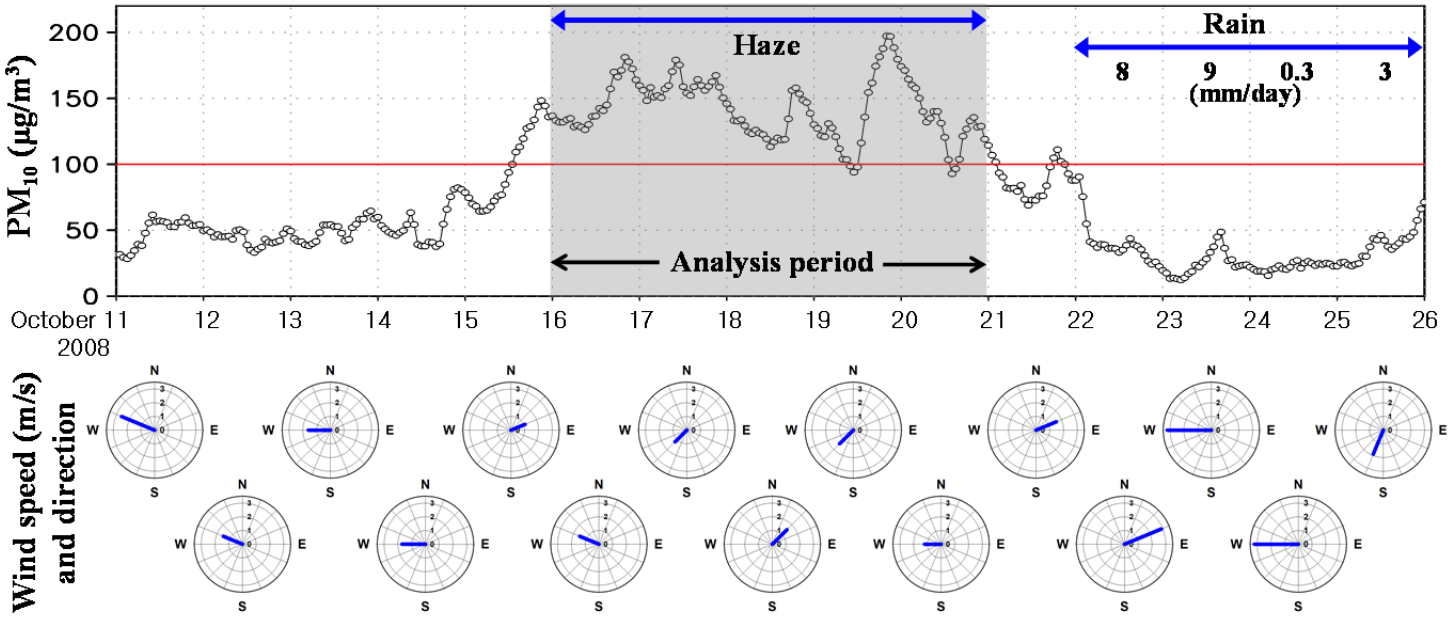

Fig. 4.1. Time series of hourly PM_{10} concentrations observed in Seoul, Korea during October 11–25, 2008. Red horizontal line indicates reference value of environmental control. The polar plots in lower panel denote daily wind speed and primary wind direction.

4.2. Observational data analysis

4.2.1. Synoptic meteorological conditions

Generally, the degree of air pollution over a region depends on both the amount of pollutant emissions and the weather conditions. In fact, the weather conditions can help to concentrate or disperse pollutants within a region and transport pollutants to regions distant from the emission sources (Davis and Kalkstein, 1990; Greene et al., 1999; Cheng et al., 2007a, b; Chen et al., 2008). To examine the weather conditions during the high-PM_{10} episode, the weather maps at 00 UTC on October 15–22, 2008, are displayed in Fig. 4.2. The weather maps are obtained from Korean Meteorological Administration (KMA).

As seen in Fig. 4.2, low-pressure systems are located near Hebei and Liaoning provinces over northeastern China on October 15. Ascending air currents in these low-pressure systems may induce vertical loading of locally emitted air pollutants in that region. Considering there are many industrial sources, power plants, and large cities such as Beijing, Tianjin, Shenyang, and Dalian in this area of northeastern China, the amount of air pollutants emitted from coal combustion and heavy traffic volumes could be very large.

During the period of October 15–20, most regions of the Korean peninsula are affected by a high-pressure system with its center located near to Seoul. Thus, the weather conditions in Seoul should be stable. The high-pressure system is the dominating pattern responsible for the accumulation of air pollutants. In general, the vertical structure in a surface high-pressure system makes pollutant dispersion difficult, and is therefore beneficial for the accumulations of pollutants (Chen et al., 2008). During the high-PM_{10} episode, fog was frequently observed over Korea, as well as central and southern China (see yellow dots in weather maps of Fig. 4.2), which is thought to be a haze caused by the many pollutant particles in the air.

It is noted that most high pressure occurring during October is a result of migratory anticyclones passing through the Korean peninsula within a few days. However, the high pressure in the analyzed episode remained in the vicinity of Seoul for around a week, without moving to the east. Therefore, the exceptionally stagnant high-pressure system over Korea could be the main cause of the extraordinarily long continuity of high PM_{10} levels. What factors are responsible for the long-lasting high-pressure system in Korea? A peculiar feature in the weather maps is a typhoon located over the southeast of Japan on October 19 and 20. This is Bavi, the eighteenth typhoon of 2008. It formed at 15:00 on October 19, over the sea 1500 km north-northeast of Guam, later

moving to the southeast of Japan, and finally dissipating at 21:00 on October 20 in the sea 1300 km east of Tokyo. It was a small, weak typhoon with strong winds within a 100 km radius and central minimum pressure of 992 hPa. However, it would have been sufficiently powerful to block a migratory anticyclone passing through the Korean peninsula. After the dissipation of Bavi, the PM_{10} concentrations decreased, simultaneous with the migration of the stationary anticyclone from the Korean peninsula to the East Sea on October 21. In additions to typhoon Bavi, there is a probable factor that contributes to the long-lasting high-pressure system over Korea. On October 18–21, the upper-level ridge is located on the eastern side of the Korean peninsula (Fig. 4.3). This pressure system may impede the atmospheric flow around Korea and partially contributes to blocking the passage of migratory anticyclones.

Through an analysis of weather maps, we suggest that transboundary air pollutants from northeastern China contribute to high-PM_{10} episode in Seoul. However, this is just estimation, so the movement of air pollutants from China to Korea has been investigated using satellite and lidar observations.

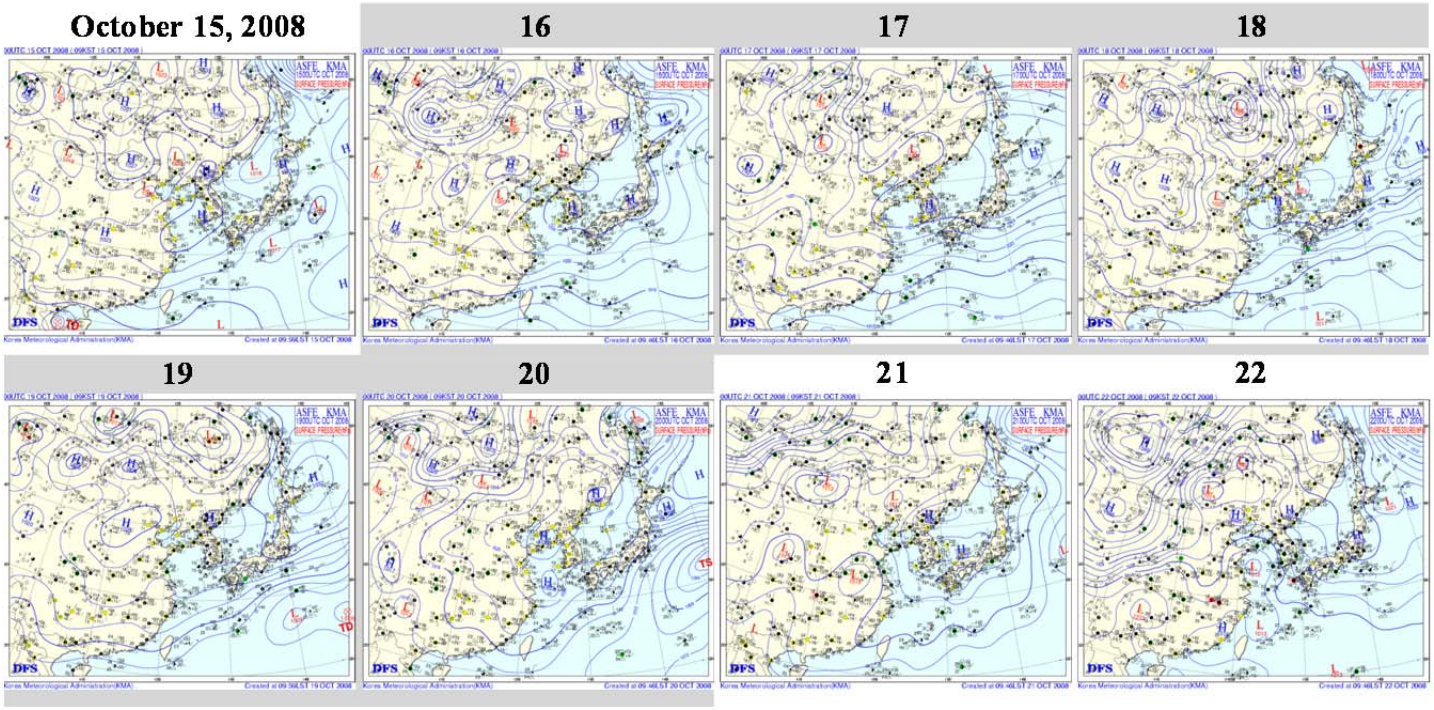

Fig. 4.2. Synoptic maps on October 15–22, 2008. Gray shaded box denotes high-PM_{10} days focused on in this study.

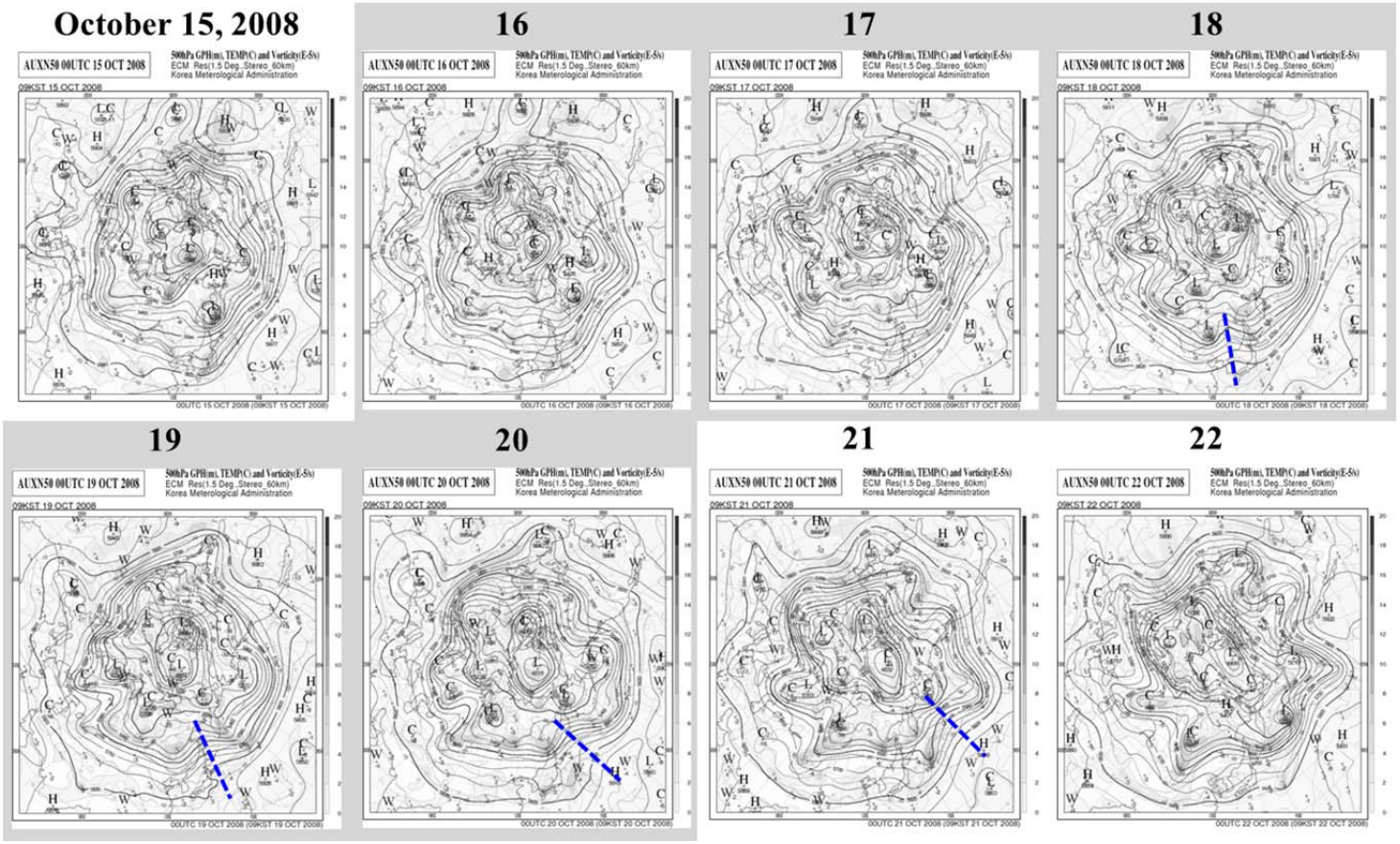

Fig. 4.3. Same as Fig. 4.2, except for 500 hPa geopotential height (solid curve) maps. Blue dotted lines in the maps denote the pressure ridges around the Korean peninsula.

4.2.2. Satellite observations and airflows

Remote sensing with satellites has been used to monitor air quality since the late 1970s, overcoming spatial and temporal limitations of surface observation networks. In particular, these observations are helpful in tracking long-range transport of air pollutants (e.g., Hutchison, 2003; Al-Saadi et al., 2005). Some studies have examined transboundary aerosols over East Asia using satellite data (Lee et al., 2007; Huang et al., 2008; Hara et al., 2009; Jung et al., 2010). In the present study, we investigate the migration of air pollutants during the high-PM_{10} episode using a dataset collected by by Moderate Resolution Imaging Spectroradiometer onboard the Terra satellite (Terra-MODIS) and Cloud Aerosol LIdar with Orthogonal Polarization (CALIOP) onboard the Cloud-Aerosol Lidar and Infrared Pathfinder Satellite Observation (CALIPSO). Terra-MODIS and CALIOP/CALIPSO products are obtained from the Giovanni website (http://giovanni.gsfc.nasa.gov/).

Figure 4.4 shows the spatial distribution of aerosol optical depth at 550 nm (AOD_{550}) from Terra-MODIS, along with horizontal wind fields at 700 hPa during October 13–22, 2008. Longitude-height cross-sections of zonal and vertical winds at 37.34°N (the same latitude as Seoul) are also presented. Zonal, meridional, and vertical wind values are obtained from the National Centers for

Environmental Prediction-National Center for Atmospheric Research (NCEP-NCAR) reanalysis (Kalnay et al. 1996). Before the high-PM_{10} episode, the region with a high concentration of aerosols (i.e., high AOD_{550}) over northeastern and eastern China is remarkable. This region matches the low-pressure system presented in the preceding analysis of the surface weather map (see Fig. 4.2). Shandong, Hebei, Jiangsu, Henan, Shanxi, and Liaoning provinces in this region are the largest contributors to PM_{10} emission in China (Zhang et al., 2009). As mentioned earlier, it is also likely to be the source region for the high PM_{10} episode in Seoul that is the focus of this study. In addition, ascending air flows from this source region are observed on the day preceding the onset of the high-PM_{10} episode. As seen in Fig. 4.4, on October 13 and 14, the strong westerlies (wind speed $\geq$ 10 m s^{-1}) near 40°N and southwesterlies along the rim of the anticyclone over southwestern China merge and descend towards the high AOD_{550} region. On October 15, the westerly along the north rim of the anticyclone located over the Shandong province converges on the Korean peninsula. These strong winds in and around the high AOD_{550} regions play an important role in the long-range transport of air pollutants, as Seoul is more than 1000 km apart from the source regions in China. On October 16 and 17, the extension of the aerosol band to the Korean peninsula is prominent, although there are some limitations in the satellite data owing to cloud contamination.

Moreover, the anticyclone moves toward Korea, inducing westerlies and descending air currents around Seoul. These pressure and wind systems may continuously contribute to the supply from China and the accumulation of air pollutants in Seoul. Until October 20, anticyclonic and inducing descendent airflows are maintained around Seoul, although on a smaller scale. On October 19–20, low-level winds become weak, which may prevent accumulated air pollutants from scattering. After the episode, with the migration of the anticyclone from the Korean peninsula, ascending air currents are detected over Seoul.

Next, it is necessary to investigate whether particulate matter spreads up to altitudes where strong westerlies dominate. Using vertical feature mask images for daytime conditions over China and Korea from CALIPSO observations, the vertical distributions of aerosols are examined (Fig. 4.5). During the period of October 12–20, 2008, CALIPSO overpasses near China and Korea at 05–06 UTC every other day. On 12–16 October, aerosol layers in the high AOD_{550} regions over northeastern China are distributed up to altitude of 3 km or higher. The aerosols that ascend to the upper layer may be transported to Seoul by the strong westerly winds discussed above. On October 18 and 20, the height of the aerosol layer near Korea decreases to 2 km altitude; this is related to the descent of aerosols under the stable atmospheric conditions associated with the high-

pressure system. While not shown in the figure, aerosol subtypes measured by CALIPSO before and during the episode mostly consist of polluted dust (i.e., an external mixture of dust, smoke, and urban pollution), polluted continental material (pollution emanating from continent), and dust. Categorization of the aerosol subtype is described in Omar et al. (2009). These results also suggest that aerosols during the high-PM_{10} episode are transported from source regions over northeastern China.

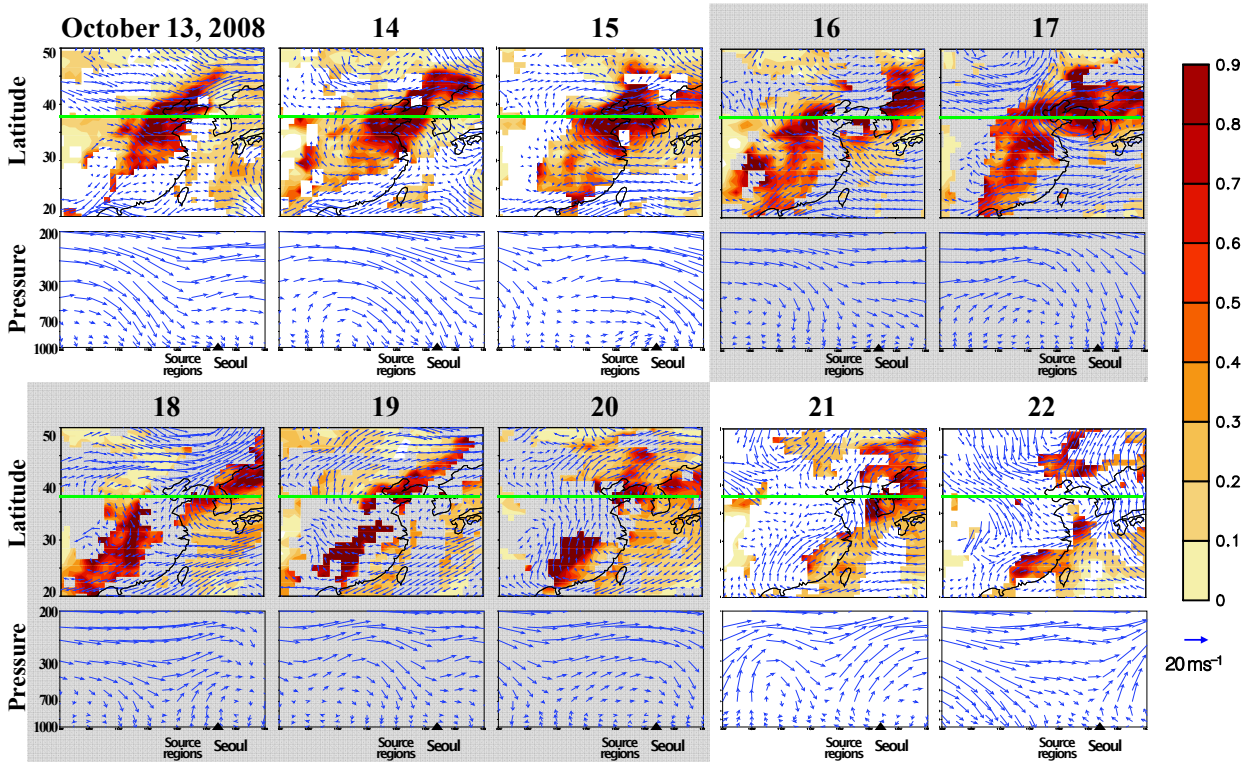

Fig. 4.4. Spatial distributions of the Terra-MODIS AOD_{550} values in October 13–22, 2008 (shaded regions). Blue arrows denote 700 hPa horizontal (panels in the first and the third rows), zonal and vertical winds (panels in the second and the fourth rows). Green horizontal lines over panels in the first and the third rows indicate the latitude, 37.34°N at which Seoul is located.

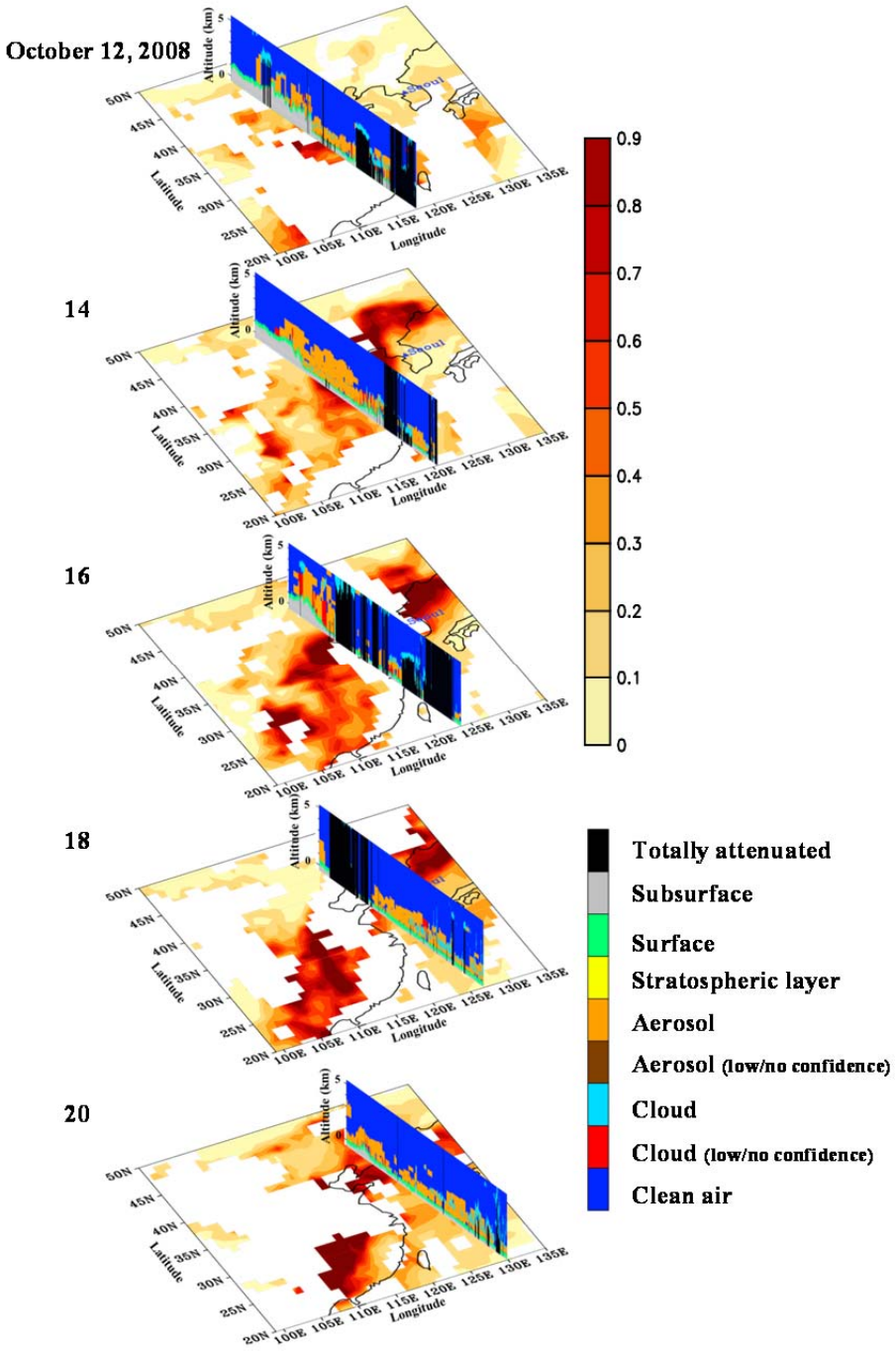

Fig. 4.5. Vertical feature mask images for daytime conditions over China and Korea from CALIPSO observations on October 12, 14, 16, 18, and 20, 2008.

4.2.3. Lidar observations

We have briefly examined the vertical structure and subtype of aerosols observed in Seoul during the analysis period through CALIPSO data. However, it is difficult to accurately draw conclusions because CALIPSO does not overpass Seoul directly on most of the high-PM_{10} days. Therefore, we use a lidar dataset that can continuously provide similar information during the high-PM_{10} episode. Lidar is widely used to retrieve the vertical profiles and optical properties of aerosols (Chazette et al., 2005; Xie et al., 2008; Uno et al., 2009; Yoon et al., 2010; Winker et al., 2010). Aerosol optical properties in Seoul are continuously observed with the Raman and Backscatter Lidar system located at Seoul National University (37.46°N, 126.95°E). Observation results, including the extinction coefficient, backscatter coefficient, lidar ratio, and depolarization ratio are also available at National Institute for Environmental Studies' (NIES) Lidar Network homepage (http://www-lidar.nies.go.jp/, Murayama et al., 2001).

The vertical structure and particle type of aerosols over Seoul are examined from the images of attenuated backscatter coefficient and depolarization ratio profiles at 532 nm observed in October 2008 (Fig. 4.6). The attenuated backscatter coefficient is frequently used to identify vertical distribution of aerosols, because it is approximately negatively correlated with

aerosol size; the value decreases as the size increases, and vice versa (Sakai et al., 2002; De Tomasi et al., 2003; Noh et al., 2007; Badarinath et al., 2010). Figure 4.6a shows that the attenuated backscatter coefficient below the boundary layer is significantly lower during the high-PM_{10} episode compared with the coefficient before and after the episode, which means that the aerosol concentrations are very high during the high-PM_{10} episode. A thick aerosol layer is distributed to an altitude of 0.8–2.5 km during this period. From the profiles of depolarization ratio shown in Fig. 4.6b, most of the aerosol is estimated to be small particulate pollution, not dust. The depolarization ratio is a useful optical parameter in distinguishing non-spherical coarse dust and spherical fine pollution aerosols (Yoon et al., 2010; Kim et al., 2011). A higher proportion of spherical particles results in a smaller value, and more spherical-shaped particles are typically associated with urban or industrial pollution (Burton et al., 2012). According to a preceding study by Yoon et al. (2010), the depolarization ratio is about 10–20% in yellow dust cases and below 5% in pollution cases. The depolarization ratio is 1–5% during the high-PM_{10} episode, demonstrating that the small pollution particle is dominant in this case and supporting the hypothesis that these particles come from industrial regions in China, as seen in satellite data.

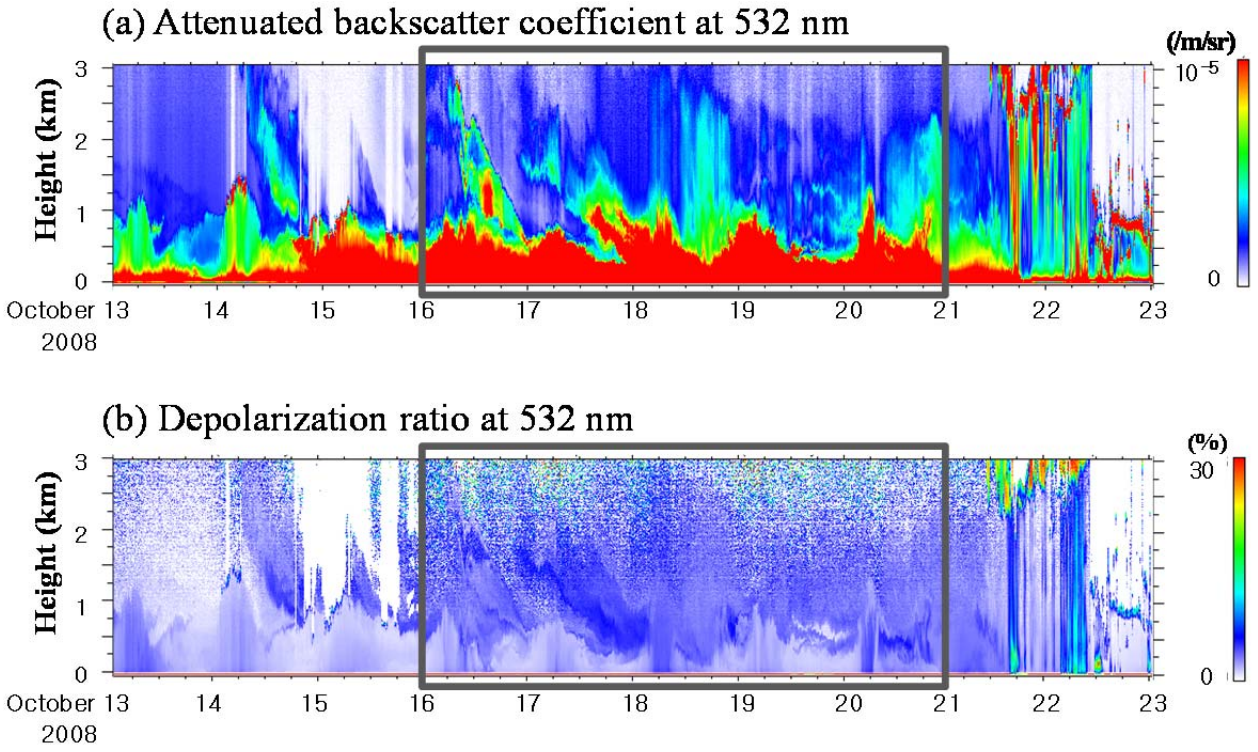

Fig. 4.6. Images of (a) attenuated backscatter coefficient, and (b) depolarization ratio profiles at 532 nm for October 11–25, 2008, observed from NIES lidar in Seoul. Gray boxes denote the high-PM_{10} days focused on in this study.

4.2.4. Station observations and back trajectory analysis

From the analysis of satellite and lidar observations, it seems that transboundary aerosols from China may have caused the high-PM_{10} episode in Seoul. However, it is still not sufficient to reach a conclusion about the linkage of air pollutants from China source regions and the Seoul area. To draw a conclusion more definitively, we apply a back trajectory analysis method and analyze the changes in PM_{10} levels in the source regions in China. The wind back trajectory analysis is commonly used in identifying source regions and pathways of aerosols (Stohl, 1996, 1998; Borge et al., 2007; Ariano et al., 2008; Lee et al., 2011). In this study, we calculated the 96-hour back trajectories of each high-PM_{10} day using the FLEXTRA trajectory model (Stohl et al., 1995; Stohl and Seibert, 1998). Temperature, 3-dimensional wind, specific humidity, and surface pressure are used as input data. More detailed information about back trajectory analysis method using in this study can be found in Lee et al. (2011).

Back trajectories are plotted in Fig. 4.7a. The end points of each trajectory are located near the industrial regions in the eastern and northeastern China (e.g., Shandong, Jiangsu, and Anhui provinces), showing that those industrial regions are possible source regions of the high PM_{10} in Seoul. As appears in the 3-day

back trajectories of the period October 16–18, airflows move from eastern China to northeastern China before the onset and early stages of the high-PM_{10} episode. This result coincides with preceding air current analysis; airflows move northeastward and approach the Korean peninsula along the rim of a migratory anticyclone. Back trajectories of October 19 and 20 show circular patterns around Seoul. This result also corresponds with that of the preceding analysis, showing a stagnation of high pressure over the Korean peninsula during the high-PM_{10} episode.

Since 2000, a daily air pollution index (API) and air quality levels have been monitored in many cities in China (Chan and Yao, 2008). To verify the change in PM_{10} levels of the source region in China, 17 API monitoring stations located near to the back trajectories are chosen (Fig. 4.7a). These are Dalian, Yantai, Jinan, Qingdao, Weifeng, Tai'an, Rizhao, Jining, Lianyungang, Zaozhuang, Kaifeng, Wuhu, Yangzhou, Ahenjiang, Nanjing, Heifei, and Suzhou. Daily PM_{10} concentrations were derived from the APIs using the following equation:

$$PM_{10} = \left[(API - API_{low})/(API_{high} - API_{low})\right] \times \left(PM_{10_{high}} - PM_{10_{low}}\right) + PM_{10_{low}}.$$

Where API_{high} and API_{low} represent API grading limits that are lower and

higher than a given API value, respectively. $PM_{10_{high}}$ and $PM_{10_{low}}$ denote the PM_{10} concentrations corresponding to API_{high} and API_{low}, respectively. For instance, $PM_{10_{high}}$= 150 and $PM_{10_{low}}$= 50, when API_{high}= 100 and API_{low}= 50, $PM_{10_{high}}$ = 250 and $PM_{10_{low}}$ = 150, when API_{high} = 150 and API_{low} = 100, and so on. The details of calculating PM_{10} concentrations from APIs are described in Qu et al. (2010). The change in calculated PM_{10} level is plotted in Fig. 4.7b. The mean PM_{10} concentration level of the 17 API stations in source regions is seen to rapidly increase from October 12, reaching its peak on October 15, a day before onset of the high-PM_{10} episode in Seoul. This result supports the hypothesis that high PM_{10} concentrations in Chinese source regions are closely related to the high-PM_{10} episode in Seoul.

(a) 96 hours back trajectory

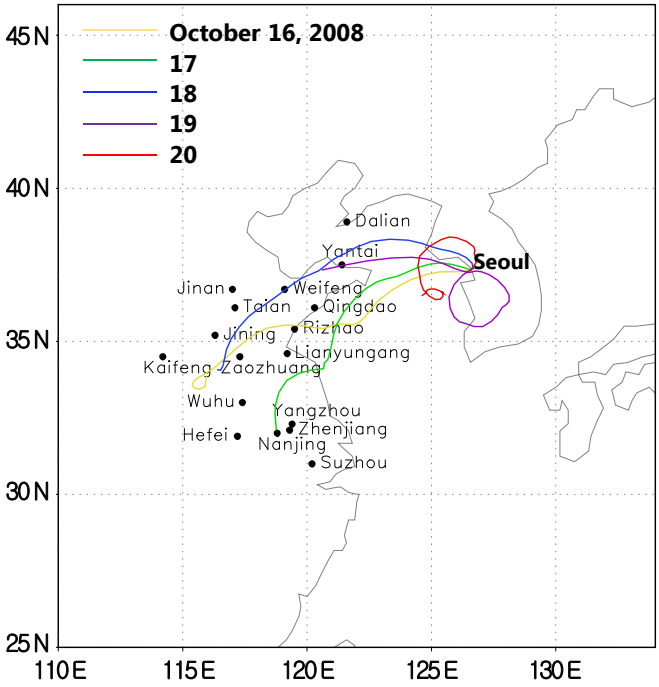

(b) PM_{10} concentration in source region

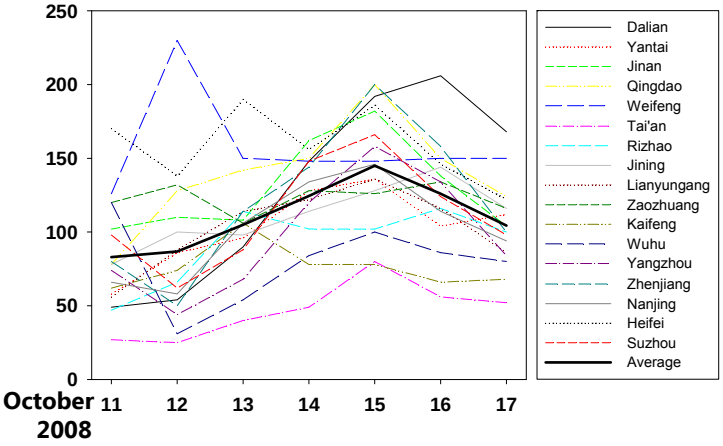

Fig. 4.7. (a) 96-hour back trajectory analysis during October 16–20, 2008, originating in Seoul, produced with FLEXTRA model. (b) Time series of PM_{10} concentration observed at the stations located near the back trajectories in (a).

4.2.5. Low tropospheric stability

Atmospheric stability in the lower troposphere is another important meteorological factor that governs mixing and the accumulation of air pollutants. Finally, we examine the mixing layer and surface inversion layer to identify the low level stability during the high-PM_{10} episode. The height of the mixing layer essentially governs the vertical mixing of atmospheric pollutants (Beyrich, 1995), and it is commonly used to estimate the dilution of pollutants released within the boundary layer (Seidel et al., 2010). It can be indicative of a transition from an underlying region of less stability to overlying more stable region, because it is a consequence of strong vertical mixing generated by convection (Kaimal et al., 1976; Shaw et al., 2007; Seidel et al., 2010). Furthermore, the surface inversion layer is a meteorological parameter relevant to the degree of air pollution. It is noted that the surface inversion layer develops in the late afternoon when there are clear skies and is dissolved by warm air from the heated ground in the morning. Emitted pollutants are trapped beneath this inversion layer during the nighttime because the lower atmosphere is very stable due to the inversion of air temperatures (Baumbach and Vogt, 2003).

The mixing layer and surface inversion layer depth are calculated using upper-air observations from radiosonde. Radiosonde was launched from Osan

(37.09°N, 127.03°E) located 53.8 km south of Seoul. We use the data observed at 06 UTC and 00 UTC in the calculations of mixing and inversion layer depth, respectively. The former and the latter are highest in the daytime and early morning, respectively. We plot the vertical profile of potential temperature (upper panel in Fig. 4.8) and air temperature (lower panel) for October 11–25, and then determine mixing and inversion layer depth of each day from the maximum vertical gradient. The 5-day mean values of mixing and inversion layer depth before, during, and after the high-PM_{10} episode are presented in Table 4.1. The low-level winds are also presented; they are relevant to dynamic stability of atmosphere.

During the high-PM_{10} episode, the mean mixing layer depth is lower and the inversion layer depth is higher, compared with periods before and after the episode. In addition, the winds in the lower troposphere during the episode are weak and calm. The shrinking of mixing layer during high-PM_{10} episode may prevent dilution of emitted pollution with clean air from the upper atmosphere. Furthermore, enhanced atmospheric stability due to the expansion of the inversion layer and reduction of wind speed in the lower troposphere may assist in the accumulation of transboundary air pollutants. All of these distinguishing meteorological fields associated with low-level stability act together to make

favorable conditions for the maintenance of high levels of PM_{10} during that period.

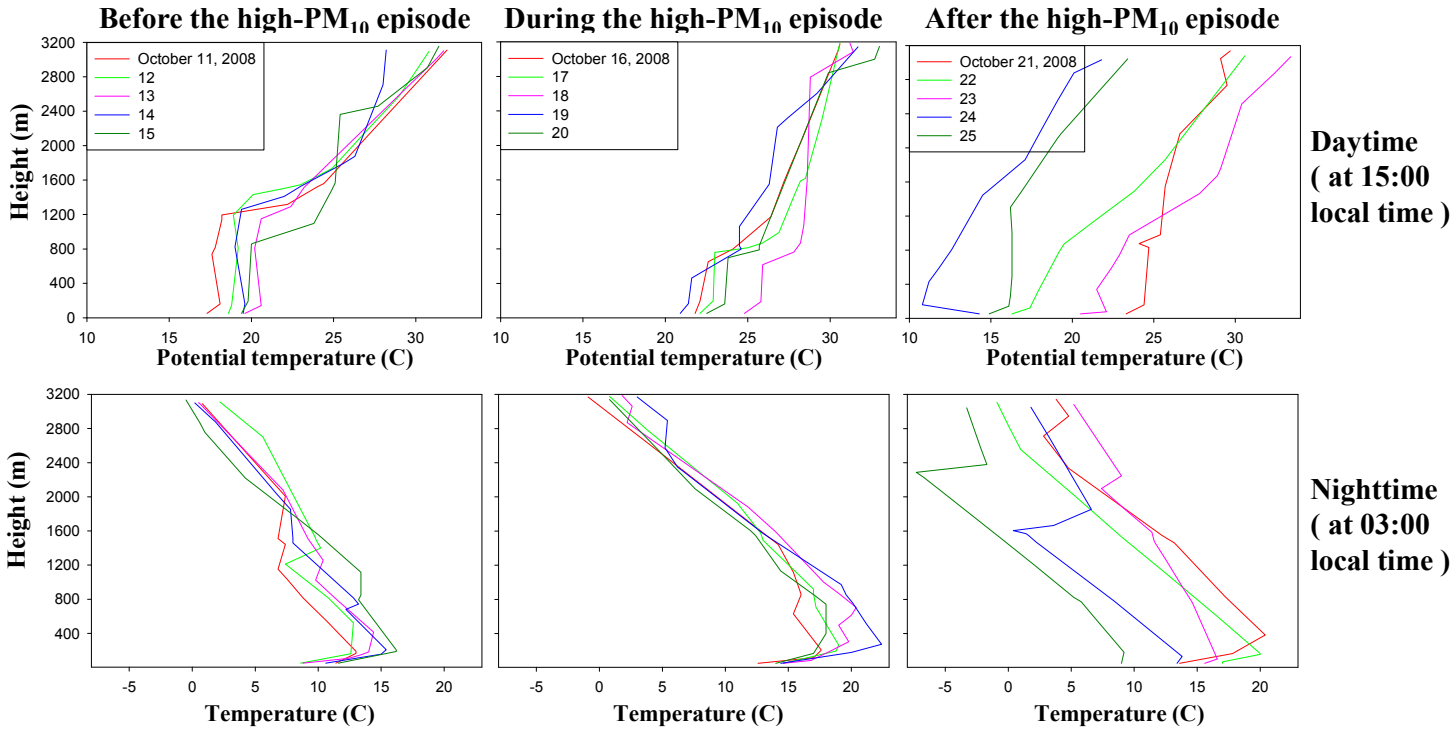

Fig. 4.8. Potential temperature (upper panels) and air temperature (lower panels) profile before (left panels), during (middle panels), and after (right panels) the high-PM_{10} episode.

Table 4.1. Mean mixing layer depth, surface inversion layer depth and wind speed in the lower atmosphere during October 11–25, 2008.

	Before the high-PM_{10} episode (October 11-15, 2008)	During the high-PM_{10} episode (October16-20, 2008)	After the high-PM_{10} episode (October 21-25, 2008)
Mean mixing layer depth (m)	1132.40	637.40	1104.80
Mean inversion layer depth (m)	308.80	439.80	193.00
Mean wind speed in lower atmosphere (m/s)	5.14	3.60	9.13

4.3. Atmospheric diffusion modeling

4.3.1. Overview of CALPUFF modeling system

In the previous chapters, we identified source regions of high- PM_{10} level in Seoul and clarified the possible mechanism of air pollutant migration from source regions to Seoul. By back trajectory modeling starting from Seoul, we inversely estimate the most source regions are large cities and industrial complexes over the northeastern and central China. This estimation has some limitation, because emissions and depositions of air pollutants along the trajectories are not considered. Furthermore, we indirectly estimate the related meteorological conditions by analyzing several observational dataset. This estimation has also its own problem, because migration of air pollutants and movement of air parcels are separately observed. We only guess that air pollutants are transported by air currents. For these reason, we verify the transportation of air pollutants from source regions to Korea by atmospheric diffusion modeling in this chapter.

The California Puff (CALPUFF) dispersion modeling system is a guideline model for regulatory use proposed by the United States Environmental Protection Agency (U.S. EPA) and is a non-steady-state Gaussian puff model (Scire et al., 2000a, b). The CALPUFF model is widely used in air quality

research due to its accuracy and reliability (Levy et al., 2002; Song et al., 2006, 2008; Hao et al., 2007; Yang et al., 2007; Abdul-Wahab et al., 2011). Especially, the CALUFF has superiority in predicting plume dispersion over a coastal region and complex terrain compared with previous dispersion models, such as Industrial Source Complex Short Term (ISCST), AERMOD, and HYSPLIT (Fisher et al., 2003). It is also suitable for predicting long-range transport and for short-range applications involving complex and non-steady-state flows (Abdul-Wahab et al., 2011). In addition, CALPUFF can model emissions from a wide range of source types (e.g., point, line, and volume sources).

CALPUFF modeling system includes three main components: CALMET, CALPUFF, and CALPOST. CALMET is a meteorological modeling package for developing hourly wind and temperature fields with various micrometeorological parameters on a three-dimensional gridded domain. The standard inputs to CALMET contain geophysical data (e.g., terrain elevations, land use, coastline) and available meteorological data (hourly surface observations, twice-daily sounding profiles, hourly precipitation data, three-dimensional data from prognostic models, such as MM5, WRF, RAMS, etc.). CALPUFF is a Gaussian puff-based transport and dispersion model with chemical removal, wet and dry deposition, complex terrain algorithms, building downwash, plume fumigation, and other effects. The CALMET outputs and emission inventory are the inputs to

CALPUFF. CALPOST is a postprocessor for the CALPUFF outputs, such as meteorological fields, concentrations and deposition fluxes. Fig. 4.9 shows the program elements in the CALPUFF modeling system and input dataset.

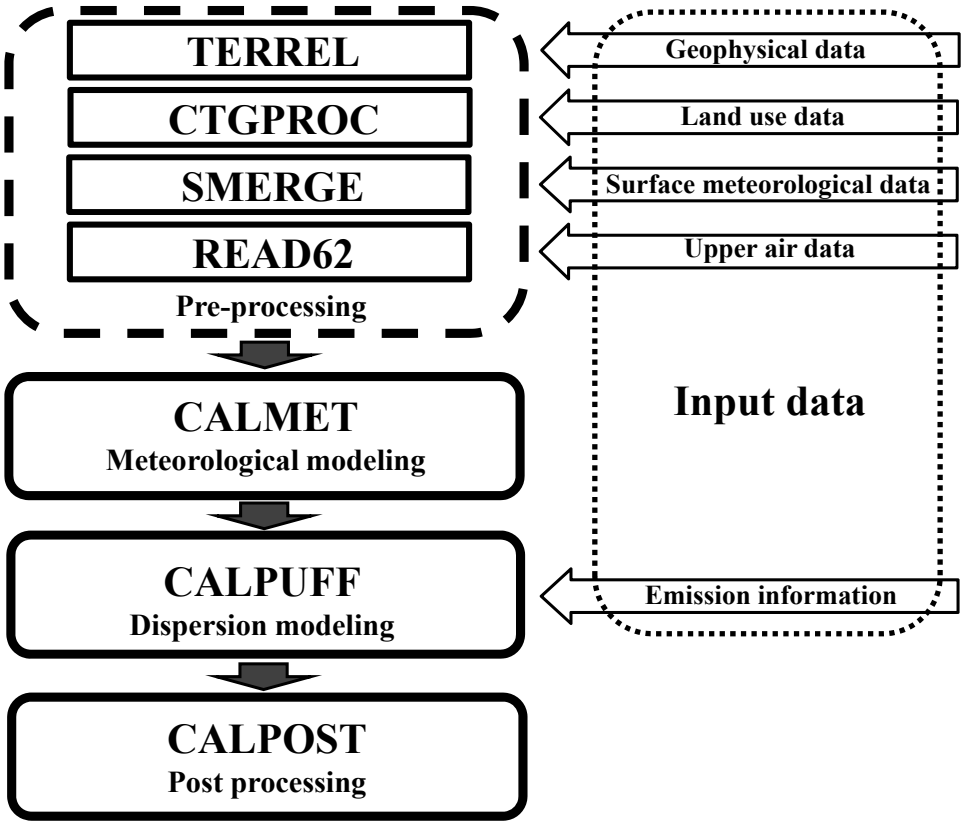

Fig. 4.9. Overview of the program elements in the CALPUFF modeling system (adopted and modified from Scire et al., 2000a,b).

4.3.2. Modeling configuration and input data

Detail information of modeling configuration is indicated in Table 4.2. The modeling domain was arranged as a 200 × 200 grid with a 10-km horizontal resolution. The origin of projection is Seoul and the modeling domain covers the east China and Korean peninsula. The coordinate system was converted to Lambert Conical Projection grid. The 12 vertical layers were used into the CALMET processing, the top of the domain being 5200 m, and the lowest layer with height of 20 m. The modeling period is four days, from October 14, 2008, 00:00 KST to October 18, 2008, 00:00 KST.

We used Shuttle Radar Topography Mission with a horizontal grid spacing of 30 arc seconds (SRTM 30) data for terrain elevation data and Global Land Cover Characteristics (GLCC) with 1-km horizontal resolution for land use data. Modeling domain with terrain elevation is shown in Fig. 4.10. The input meteorological data for CALMET is obtained from 2 surface (e.g., Seoul and Pohang) and 35 sounding observation stations over Korea and China regions. Emission sources are set up as point sources of Beijing (931.7 km west and 259.4 km north from Seoul), Qingdao (588.1 km west and 163.7 km south from Seoul), and Shanghai (482.4 km west and 709.3 km south from Seoul) (Fig. 4.10). To identify the source region of high PM_{10} in Seoul, prime cities of north

eastern, central eastern, and south eastern China are chosen as point sources. The PM_{10} emission rate is 4000 g s^{-1} in all point sources.

Table 4.2. Detail information of modeling configuration.

Origin of projection	Latitude	37.57N
	Longitude	126.97E
Grid origin (reference point)	X (Easting)	-1500 km
	Y (Northing)	-1000 km
Grid spacing (Δx)		10 km
Domain size	Nx (no. of x grid cells)	200
	Ny (no. of y grid cells)	200
Projection		Lambert Conformal Conic (LCC)
Nz (no. of vertical layers)		12
Cell face heights (m)		0, 20, 40, 80, 160, 300, 600, 1000, 1500, 2200, 3000, 4000, 5200
Time zone		UTC+0900
Modeling period		October 14, 2008, 00:00 KST – October 18, 2008, 00:00 KST
Continent/Ocean		Asia
Geoid-Ellipsoid/Datum		Korean Geodetic System 1995 :WGS 84

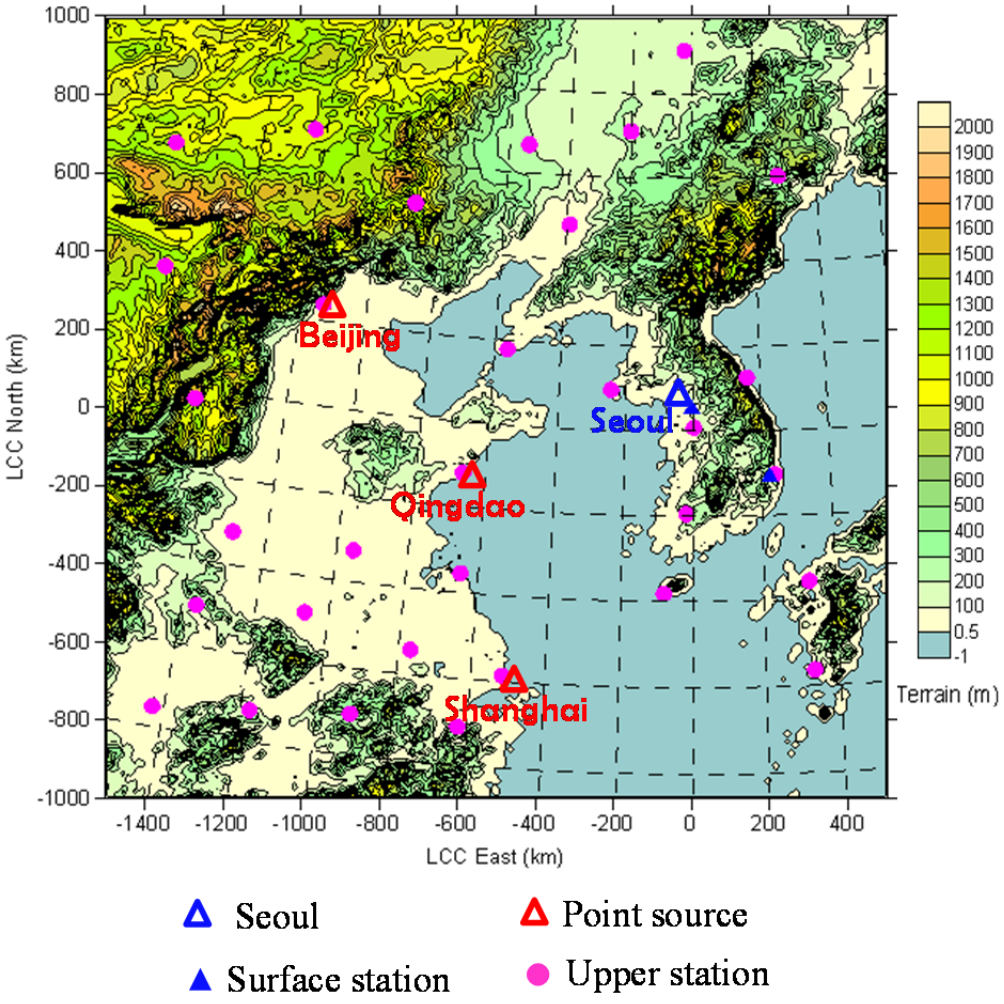

Fig. 4.10. Modeling domain with terrain elevation, point sources (Beijing, Qingdao, and Shanghai), receptor (Seoul), surface and upper stations.

4.3.3. Dispersion of particulate matters originating from China to Korea

For the spatial distribution of simulated concentrations for the study period, CALPOST was used to plot the contours. Fig. 4.11 presents the predicted PM_{10} concentration values and wind vectors for each time step. On October 14, northwesterly is prevailed around the point sources. Aerosol plumes emitted from each point source began to move southeastward along the northwesterly. The center of anticyclonic airflow is located at 1000 km west from Shanghai. On October 15, the center of anticyclone slightly moved northeastward and induced northeasterly around Shanghai. The direction of aerosol plume dispersion in Shanghai is changed from eastward to westward and is spread to China's interior. Aerosol plumes emitted from Beijing and Qingdao are continuously spread eastward and reached over the West Sea near the Korean peninsula. On October 16, 09:00 KST, aerosol plumes from Beijing and Qingdao merged and arrived in Korea along the strong northwesterly. At 21:00, aerosol plume is extended into Seoul. On the other hand, aerosol plume from Shanghai is spread further up into inland China by the easterly induced the southern rim of migratory anticyclone. On October 17, aerosol plume transported from Beijing and Qingdao covered the whole central and northern region of Korean peninsula.

The result of CALPUFF dispersion modeling shows well the air pollutant

migration pattern from north eastern and central eastern China to Korea before and early stage of high- PM_{10} episode in Seoul. It also well coincide with previous observational analysis. With this, source regions of high PM_{10} in Seoul and transport route of PM_{10} from China to Korea are confirmed more accurately.

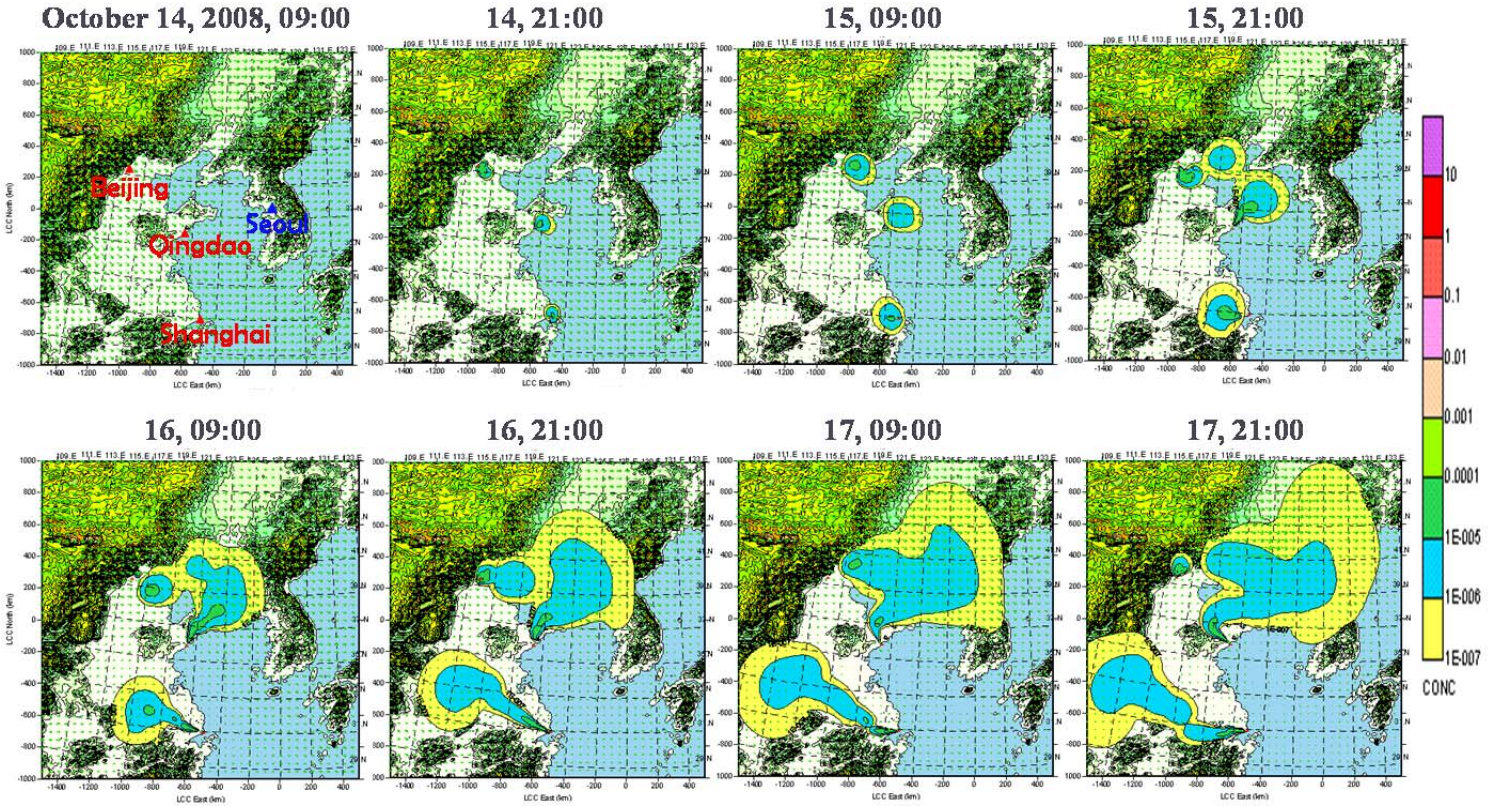

Fig. 4.11. Horizontal distribution of predicted PM_{10} concentrations (shaded, μg m3) and wind vectors (arrows, m s^{-1}) from October 14, 2008 to October 17, 2008.

4.4. Other cases

In the previous paragraphs, we investigated representative high-PM_{10} episode in 2008. We presented possible mechanism of long-lasted high-PM_{10} level in Seoul by close analysis of several dataset and atmospheric diffusion modeling. However, it is not sufficient to generalize the mechanism from only one case. We additionally investigated some other high-PM_{10} cases in recent years and tried to find similarities among them.

Firstly, high-PM_{10} episode during January 12-20, 2013 are analyzed. The levels of PM_{10} concentration are displayed in Fig. 4.12. From 13:00 on January 12, the PM_{10} concentration begins to increase above the environmental control standard value (100 μg m^{-3}), and reaches the first peak, 225.0 μg m^{-3} at 20:00. Following this, it shows a slight decreasing tendency until 07:00 on January 14. From the 08:00 on 14, the PM_{10} concentration increases again and reaches the second peak at 18:00 on January (200 μg m^{-3}). After the snow on 16, the PM_{10} concentration drops below 100 μg m^{-3}. However, it increases again up to 168 μg m^{-3} at 14:00 on 17, and reaches the final peak (173 μg m^{-3}) at 04:00 on January 20. It drops sharply below 50 μg m^{-3} after rain events on January 21 and 22. During the high-PM_{10} episode, haze was observed all over Seoul.

Synoptic maps during January 10–19, 2013 are laid out in Figs 4.13 and 4.14. Like the high-PM_{10} episode in 2008, high-PM_{10} levels are occurred in China source regions and low-pressure systems are located near Hebei and Liaoning provinces over northeastern China before the onset of high-PM_{10} episode in Seoul. Another similar feature in weather maps is the East China Sea cyclone on 14 and 15. Like the typhoon Bavi of case in 2008, this extratropical cyclone plays some role in blocking a migratory anticyclone passing through the Korean peninsula. After the dissipation of extratropical cyclone, the PM_{10} concentrations decreased, simultaneous with the migration of the stationary anticyclone from the Korean peninsula to the East Sea on January 16.

Fig 4.13 and 4.14 also show the distributions of the Terra-MODIS AOD_{550} values, 700 hPa horizontal winds, and zonal and vertical winds at 37.34°N. Before the high-PM_{10} episode, the region with a high concentration of aerosols over southeastern China is remarkable. This aerosol band extends with the strong westerlies during the episode. In addition, ascending air flows from the source region are observed on the day preceding the onset of the high-PM_{10} episode. The remarkable feature from horizontal wind maps is that the variation of PM_{10} concentration is closely related to the wind flow patterns around Korean peninsula. During the episode, PM_{10} level temporally decreases when the wind

flows changes from westerlies to northerlies. These northerlies may help the aerosols to move seawards.

Secondly, we analyzed the high-PM_{10} episode in February 2-8, 2011. The levels of PM_{10} concentration begins to increase above 100 μg m^{-3} from 03:00 on February 2, and continuously the high-PM_{10} level during the episode (Fig. 4.15). The extension of aerosol band from China to Korea is detected from the distribution of Terra-MODIS AOD_{550} values (Figs 4.16 and 4.17). On February 2, high-PM_{10} level occurs in Seoul, when the wind flows around Korean peninsula changes from northwesterly to westerly (Fig. 4.16). Migratory anticyclone moves from southeastern China to Korean peninsula during the episode. The wind flows again changes from westerly to northwesterly after a migratory anticyclone passing through the Korean peninsula in the latter stage of episode. The PM_{10} level decreases due to these wind and pressure changes.

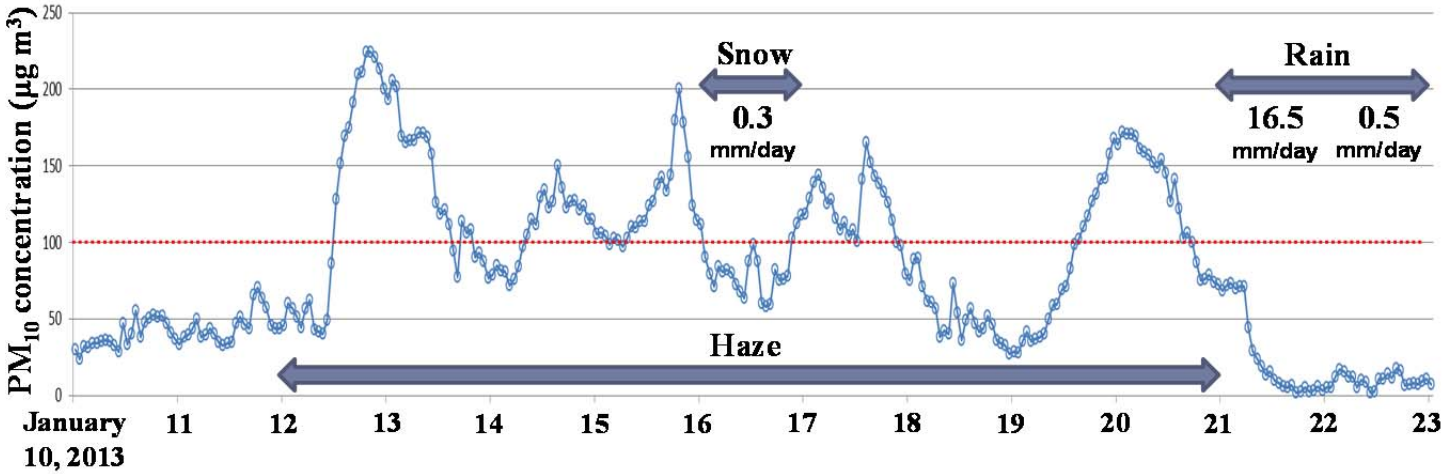

Fig. 4.12. Time series of hourly PM_{10} concentrations observed in Seoul, Korea during January 10–23, 2013. Red horizontal line indicates reference value of environmental control.

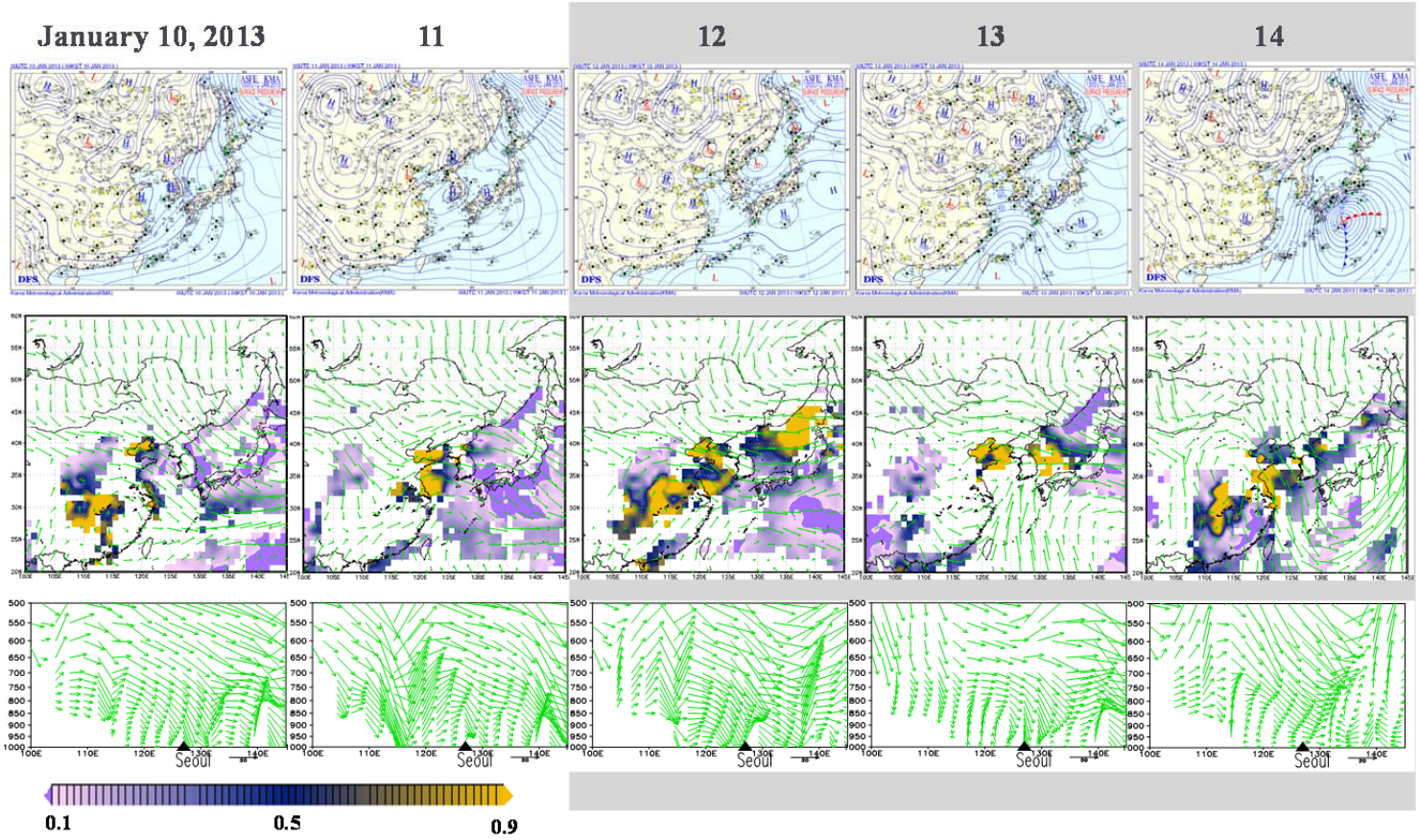

Fig. 4.13. Synoptic maps (top row), spatial distributions of the Terra-MODIS AOD_{550} values (shaded regions in middle row), 700 hPa horizontal winds (arrows in middle row), and zonal and vertical winds at 37.34°N (arrows in bottom row) in January 10–14, 2013.

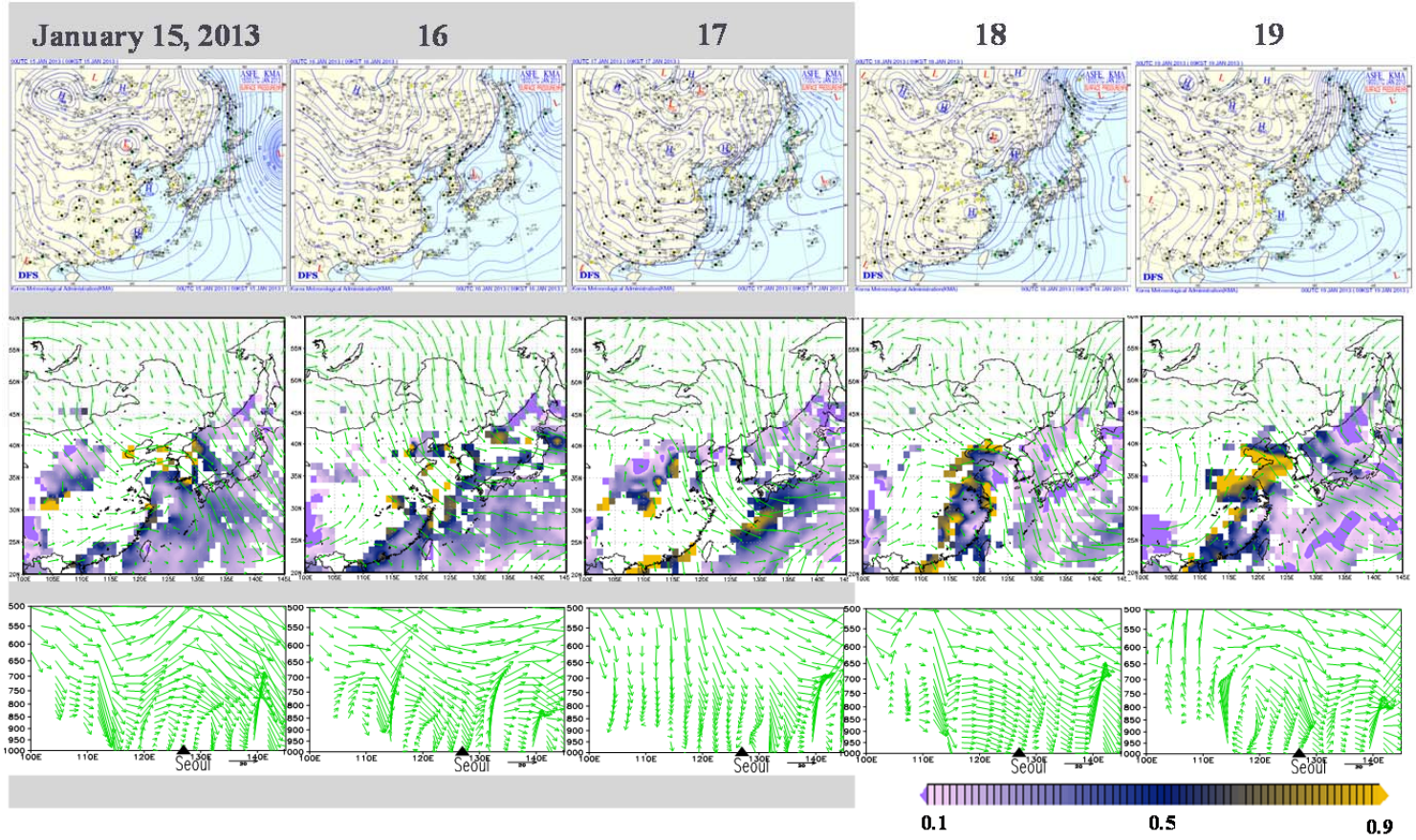

Fig. 4.14. Same as Fig. 4.13, except for in January 15–19, 2013.

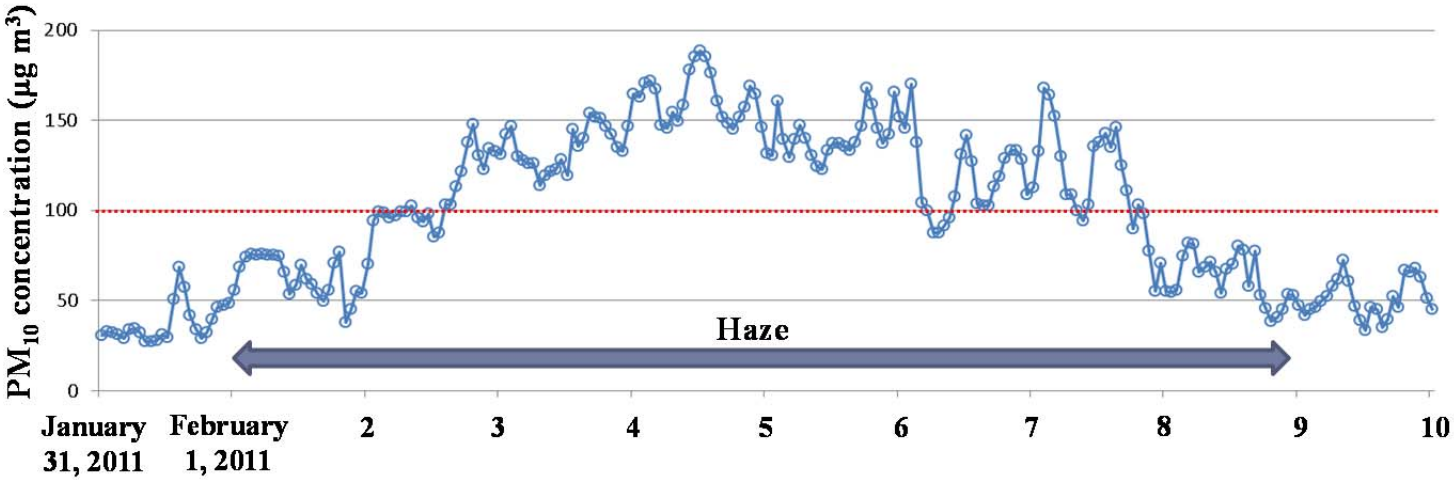

Fig. 4.15. Same as Fig. 4.12, except for from January 31 to February 9, 2011.

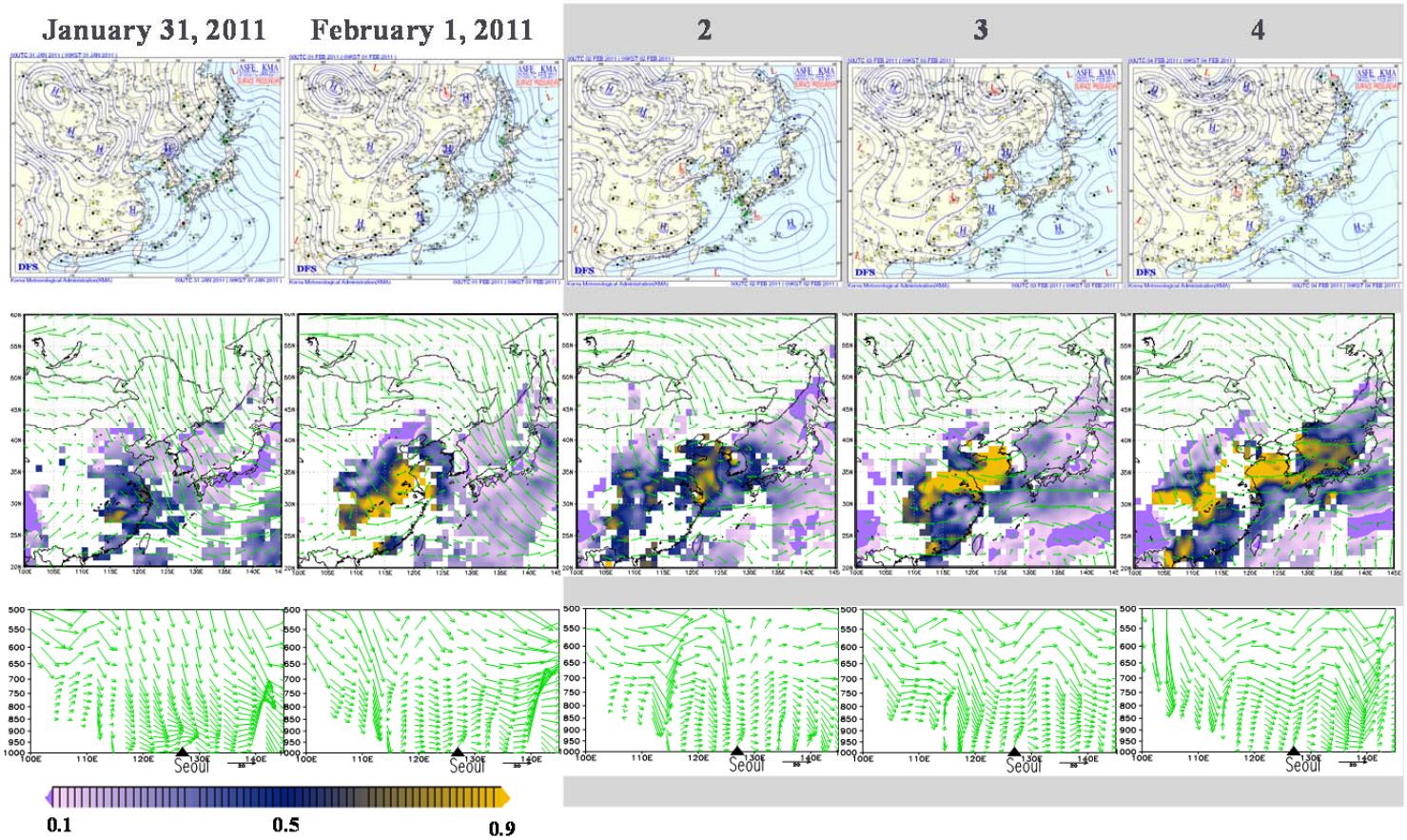

Fig. 4.16. Same as Fig. 4.13, except for from January 31 to February 4, 2011.

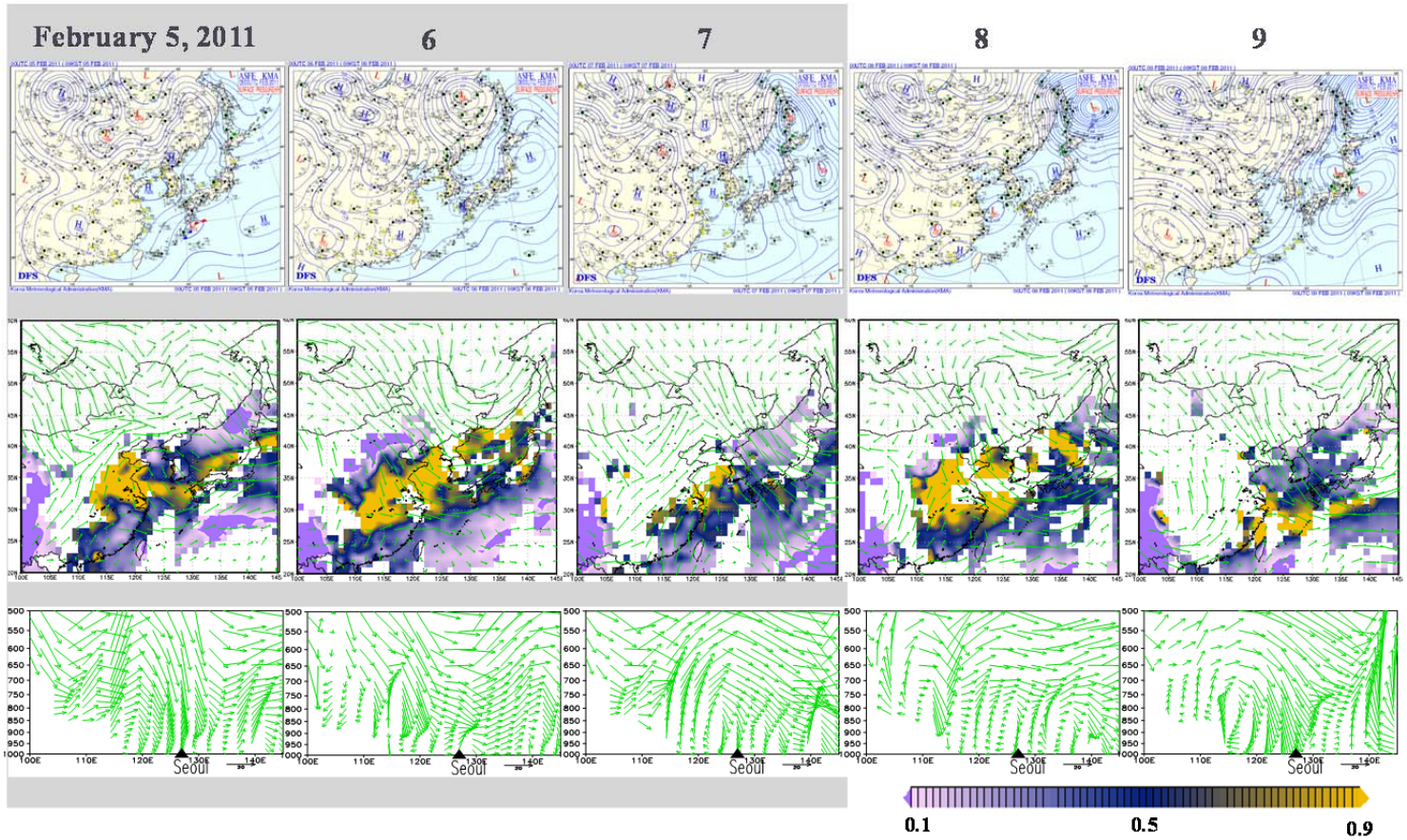

Fig. 4.17. Same as Fig. 4.13, except for in February 5–9, 2011.

5. SUMMARY AND DISCUSSION

In this study, the causes of high PM_{10} occurred in Seoul are examined by identifying source regions and clarifying related meteorological fields.

We examine the source regions and pathways of PM_{10} by back trajectory analysis and contribution of internal and external sources of PM_{10} by the clustering analysis. Results show that one local source region (local source from the Korean peninsula and the Yellow Sea) and two external source regions (major cities and industrial districts in inland China, Gobi desert area) may be of high PM_{10} levels in Seoul. Furthermore, we could also infer that transboundary pollutants of high PM_{10} levels are over twice as much as those from internal sources, especially in winter and spring seasons. Local pollutants of high PM_{10} have decreased through the efforts to reduce pollutant emission, but transboundary pollutants have not decreased.

The composite of the selected meteorological variables shows that high air temperature, light precipitation, and weak lower/upper-level wind favors high PM_{10} concentration. It is noted that these are rather dependent and dynamically coupled. Furthermore, PM_{10} pathway results suggest that we need to distinguish high PM_{10} episodes due to external sources from those due to local sources. In the present study, we were able to clarify that anomalous wind and pressure

fields are key factors to determine both occurrence and source type of high PM_{10} episodes. The prevailing meteorological patterns for local and external source types of high PM_{10} episodes are summarized in a schematic diagram (Fig. 5.1). In the case of local source type, strong anomalous high pressure over the northern region of Korean peninsula induces anomalous easterly and weakens the westerlies near Seoul, making favorable condition for accumulation of locally emitted pollutants (Fig. 5.1a). In the case of external source type, anomalous high pressure over the southern region of Korea induces anomalous westerlies and intensifies the westerlies near Seoul. Besides, anomalous low pressure over the external source region induces ascending air currents and anomalous westerly, loading pollutants on the westerlies (Fig. 5.1b). In both types, weak and calm lower wind over Korea and the surrounding area are dominant. Therefore, the spread of pollutants from the source regions occurs mostly in the upper troposphere.

The Korean peninsula is adjacent to possible sources of air pollutants such as large cities and industrial complexes in China, deserts in northern China and Mongolia, and wild fires in Russia. Serious air pollution episodes occur frequently in Seoul, Korea despite many efforts to curb locally emitted pollutants. This means that air quality in Seoul is significantly influenced by the inflow of particulate matter from external sources as well as local sources.

The present study into the high-PM_{10} episode of October 2008 shows the detailed processes by which transboundary air pollutants from China influence the air quality in Seoul. Furthermore, we also verify that the influence of China-originated air pollutants can be significantly intensified when particular meteorological conditions are prevalent. The summary of the process of the studied episode is represented simply in Fig. 5.2. Updraft of air pollutants from the source regions by ascending air currents is induced by a low-pressure system at the surface, transport by strong westerlies is induced by a high-pressure system in the upper layer, and descent to Seoul and accumulation of air pollutants occurs as a result of a stable low-level atmosphere. Combined, these are the primary causes of long-lasting high-PM_{10} levels in Seoul. This result is based on extensive analysis performed in this study using several observation datasets and atmospheric dispersion modeling. It can be concluded that meteorological conditions, such as distribution of atmospheric pressure, the movement of air currents, and the change of atmospheric stability, can play crucial roles in the occurrence and maintenance of high-concentration air pollution episodes.

Favorable meteorological conditions for transport and accumulation of transboundary air pollutants can develop any time, with thermodynamic and dynamic causes. In particular, advantageous conditions associated stagnant

anticyclones can often be formed in spring and autumn in Korea, because migratory anticyclones frequently pass by the Korean peninsula during those seasons. More specifically, migratory anticyclones travel nearby the Korean peninsula, accompanying cyclone to the rear, and sometimes remaining around the Korean peninsula for a long time due to atmospheric blocking, forming a weather condition similar to that seen in Fig. 5.2. Pollution episodes associated with this weather patterns have been addressed in some previous studies (Chun and Lim, 2004; Kim et al., 2012). Our results further imply that long-lasting air pollution episodes can occur against an overall improvement in air quality whenever suitable meteorological circumstances are prevalent. We expect that our findings will contribute to the formulation of a control strategy for air pollution and assist in the forecast of air pollution episodes in the future.

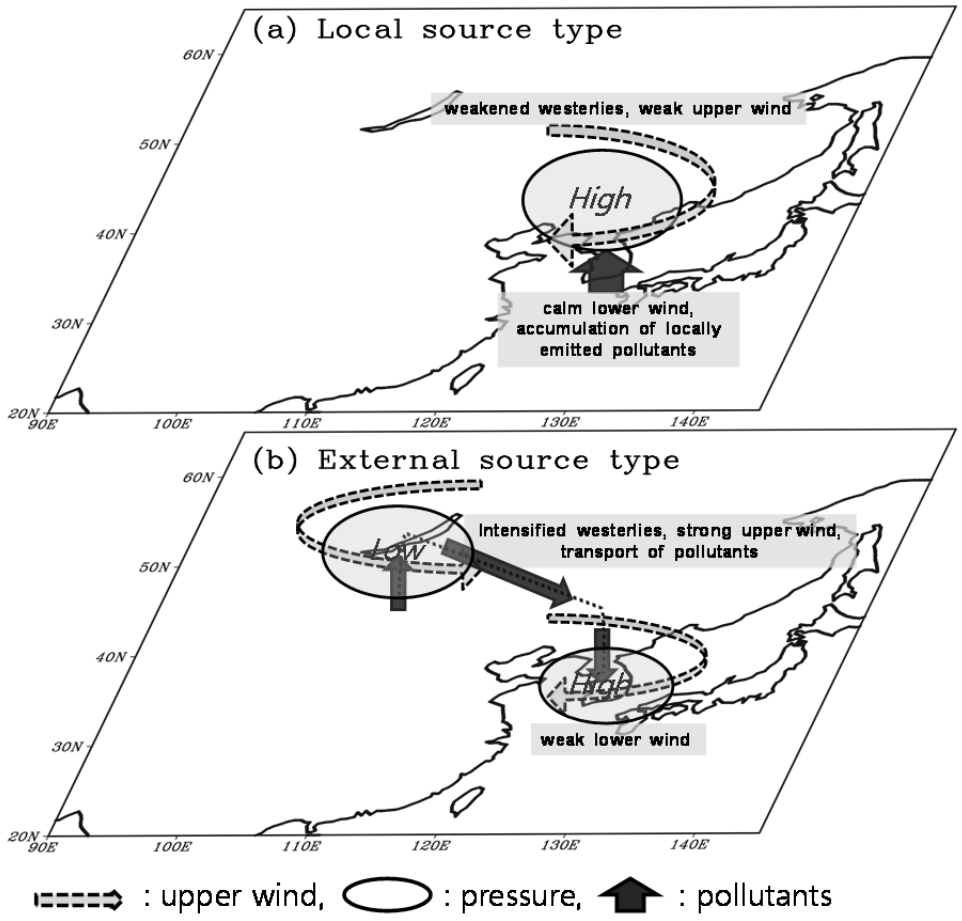

Fig. 5.1. Schematic diagram of local and external sources of high-PM_{10} episodes in Seoul, Korea.

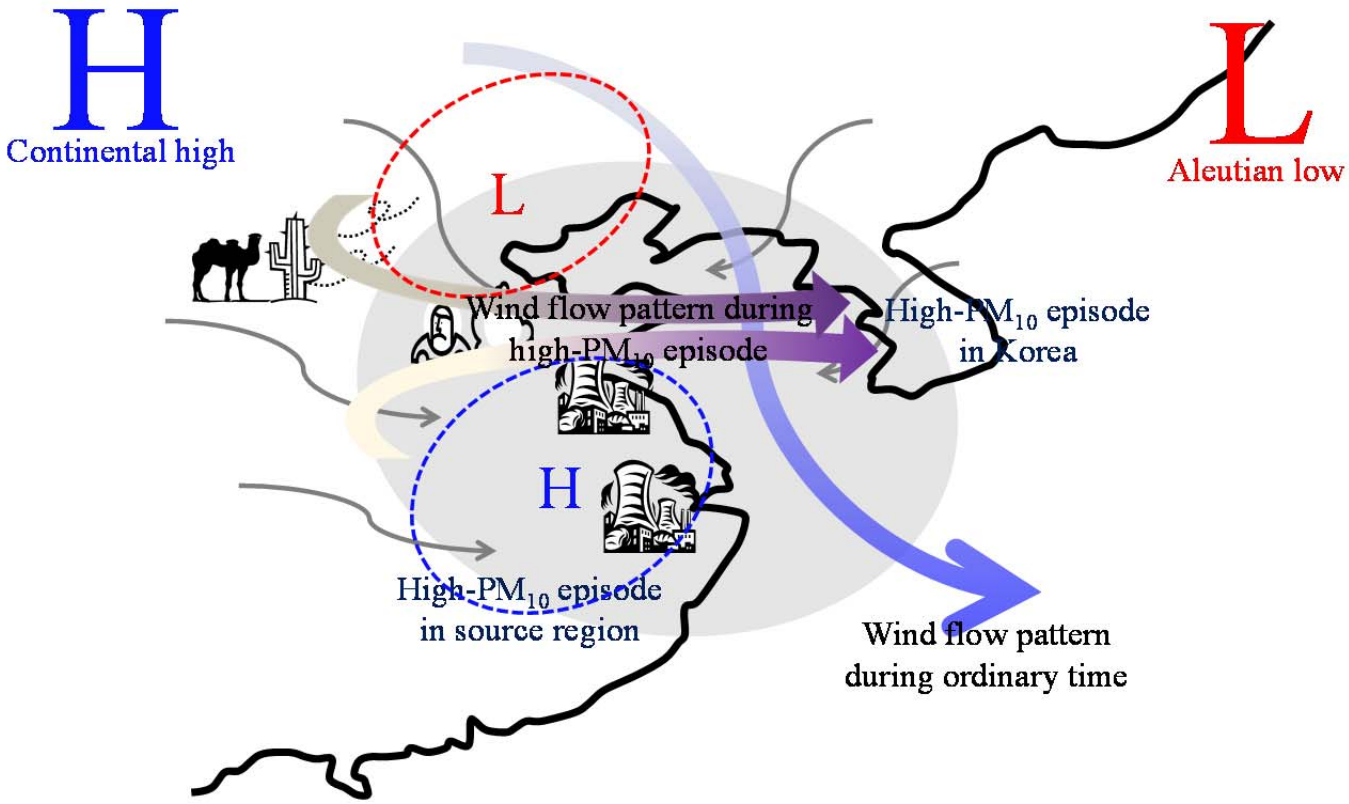

Fig. 5.2. Schematic diagram of the occurrence of the high-PM_{10} episode in Seoul, Korea.

REFERENCE

Abdul-Wahab, S., Sappurd, A., Al-Damkhi, A., 2011. Application of California Puff (CALPUFF) model: a case study for Oman. Clean Technologies and Environmental Policy 13, 177–189.

Ariano, P., Martikainen, J., Hussein, T., Valkama, I., Vehkamäki, H., Sogacheva, L., Härkonën, J., Karppinen, A., Koskentalo, T., Kukkonen, J., Kulmala, M., 2008. Analysis and evaluation of selected PM_{10} pollution episodes in the Helsinki Metropolitan Area in 2002. Atmospheric Environment 42, 3992–4005.

Badarinath, K.V.S., Kharol, S.K., Kaskaoutis, D.G., Sharma, A.R., Ramaswamy, V., Kambezidis, H.D., 2010. Long-range transport of dust aerosols over the Arabian Sea and Indian region — a case study using satellite data and groundbased measurements. Global and Planetary Change 72 (3), 164–181.

Baumbach, G., Vogt, U., 2003. Influence of inversion layers on the distribution of air pollutants in urban areas. Water, Air and soil Pollution: Focus 3, 67–78.

Beyrich, F., 1995. Mixing-height estimation in the convective boundary layer using sodar data. Boundary-Layer Meteorology 74, 1–18.

Borge, R., Lumbreras, J., Vardoulakis, S., Kassomenos, P., Rodríguez, E., 2007. Analysis of long-range transport influences on urban PM_{10} using two-stage atmospheric trajectory clusters. Atmospheric Environment 41, 4434–4450.

Burton, S.P., Ferrare, R. A., Hostetler, C. A., Hair, J. W., Rogers, R. R., Obland, M. D., Butler, C. F., Cook, A. L., Harper, D. B., Froyd, K. D., 2012. Aerosol classification using airborne High Spectral Resolution Lidar measurements–methodology and examples. Atmospheric Measurement Techniques 5, 73–98.

Chaloulakou, A., Kassomenos, P., Spyrellis, N., Demokritou, P., Koutrakis, P., 2003. Measurements of PM_{10} and $PM_{2.5}$ particle concentrations in Athens, Greece. Atmospheric Environment 37, 649–660.

Chan, C.K., Yao, X.H., 2008. Air pollution in mega cities in China. Atmospheric Environment 42, 1–42.

Chang, C.T., Tsai, C.J., 2003. A model for the relative humidity effect on the readings of the PM-10 beta-gauge monitor, Journal of Aerosol Science 34, 1685–1697.

Chazette, P., Randriamiarisoa, H., Sanak, J., Couvert, P., Flamant, C., 2005. Optical properties of urban aerosol from airborne and ground-based in situ measurements performed during the Etude et Simulation de la Qualite de l'air en Ile de France (ESQUIF) program, Journal of Geophysical Research 110, D02206. doi:10.1029/2004JD004810.

Chen, Z.H., Cheng, S.Y., Li, J.B., Guo, X.R., Wang, H.Y., Chen, D.S., 2008. Relationship between atmospheric pollution processes and synoptic pressure patterns in northern China. Atmospheric Environment 42, 6078–6087.

Cheng, C.S., Campbell, M., Li, Q., Li, G., Auld, H., Day, N., Pengelly, D., Gingrich, S., Yap, D., 2007a. A synoptic climatological approach to assess climatic impact on air quality in south-central Canada, Part I: historical analysis. Water, Air, and Soil Pollution 182, 131–148.

Cheng, C.S., Campbell, M., Li, Q., Li, G., Auld, H., Day, N., Pengelly, D., Gingrich, S., Yap, D., 2007b. A synoptic climatological approach to assess climatic impact on air quality in south-central Canada, Part II: future estimates. Water, Air, and Soil Pollution 182, 117–130.

Choi, Y.S., Ho, C.H., Gong, D.Y., Park, R., Kim, J., 2008. The impact of aerosols on the summer rainfall frequency in China. Journal of Applied Meteolorogy and Climatology 47, 1802–1813.

Chun, Y., Lim, J.Y., 2004. The recent characteristics of Asian Dust and haze events in Seoul, Korea. Meteorology and Atmospheric Physics 87, 143–152.

Damoah, R., Spichtinger, N., Forster, C., James, P., Mattis, I., Wandinger, U., Beirle, S., Wagner, T., Stohl, A., 2004. Around the world in 17 days—

Hemispheric scale transport of forest fire smoke from Russia in May 2005. Atmospheric Chemistry and Physics 4, 1311–1321.

Davis, R.E., Kalkstein, L.S., 1990. Using a spatial climatological classification to assess changes in atmospheric pollution concentrations. Physical Geography 11, 320–342.

De Tomasi, F., Blanco, A., Perrone, M.R., 2003. Raman lidar monitoring of extinction and backscattering of Africa dust layers and dust characterization. Applied Optics 42, 1699–1709.

Dockery, D.W., Pope, C.A., 1994. Acute respiratory effects of particulate air-pollution. Annual Review of Aerosol Science 29, 421–444.

Dorling, S.R., Davies, T.D., 1995. Extending cluster analysis–synoptic meteorology links to characterize chemical climates at six northwest European monitoring stations. Atmospheric Environment 29, 145–167.

Dorling, S.R., Davies, T.D., Pierce, C.E., 1992. Cluster analysis: a technique for estimating the synoptic meteorological controls on air and precipitation chemistry—method and applications. Atmospheric Environment 26, 2575–2581.

Edwards, D.P., Emmons, L.K., Hauglustaine, D.A., Chu, D.A., Gille, J.C., Kaufman, Y.J., Pétron, G., Yurganov, L.N., Giglio, L., Deeter, M.N., Yudin, V., Ziskin, D.C., Warner, J., Lamarque, J.F., Francis, G.L., Ho, S.P., Mao, D., Chen, J., Grechko, E.I., Drummond, J.R., 2004.

Observations of carbon monoxide and aerosols from the Terra satellite: Northern Hemisphere variability. Journal of Geophysical Research 109, D24202, doi:10.1029/2004JD004727.

Fang, M., Chan, C.K., Yao, X.H., 2009. Managing air quality in a rapidly developing nation: China. Atmospheric Environment 43, 79–86.

Fisher, A.L., Parsons, M.C., Roberts, S.E., Shea, P.J., Khan, F.L., Husain, T., 2003. Long-term SO2 dispersion modeling over a coastal region. Environmental Technology 24, 399–409.

Glen, W.G., Zelenka, M.P., Graham, R.C., 1996. Relating meteorological variables and trends in motor vehicle emissions to monthly urban carbon monoxide concentrations. Atmospheric Environment 96, 4225–4232.

Greene, J.S., Kalkstein, L.S., Ye, H., Smoyer, K., 1999. Relationships between synoptic climatology and atmospheric pollution at 4 US cities. Theoretical and Applied Climatology 62, 163–174.

Gyeonggi Research Institute, 2003. Estimating social costs of air pollutions and developing emission control strategies for Kyonggi-Do.

Han, Y.J., Kim, T.S., Kim, H., 2008. Ionic constituents and source analysis of $PM_{2.5}$ in three Korean cities. Atmospheric Environment 42, 4735–4746.

Hao, J., Wang, L., Shen, M., Li, L., Hu, J., 2007. Air quality impacts of power plant emissions in Beijing. Environmental Pollution 147, 401–408.

Hara, Y., Yumimoto, K., Uno, I., Shimizu, A., Sugimoto, N., Liu, Z., Winker, D. M., 2009. Asian dust outflow in the PBL and free atmosphere retrieved by NASA CALIPSO and an assimilated dust transport model, Atmospheric Chemistry and Physics 9, 1227-1239, doi:10.5194/acp-9-1227-2009.

Harrison, R.M., Yin, J., 2000. Particulate matter in the atmosphere: which particle properties are important for its effects on health. Science of the Total Environment 249, 85–101.

He, K., Huo, H., Zhang, Q., 2002. Urban air pollution in China: Current status, characteristics, and progress. Annual Reviews Energy Environment 27, 397–431.

Heo, J.B., Hopke, P.K., Yi, S.M., 2009. Source apportionment of $PM_{2.5}$ in Seoul, Korea. Atmospheric Chemistry and Physics 9, 4957–4971.

Hong, Y.C., Lee, J.T., Kim, H., Ha, E.H., Schwartz, J., Christiani, D.C., 2002. Effects of air pollutions on acute stroke mortality. Environmental Health Perspectives 110, 187–191.

Huang, J., Minnis, P., Chen, B., Huang, Z., Liu, Z., Zhao, Q., Yi, Y., Ayers, K., 2008. Long-range transport and vertical structures of Asian dust from CALIPSO and surface measurements during PACDEX. Journal of Geophysical Research 113, D23212, doi:10.1029/2008JD010620.

Hutchison, K.D., 2003. Applications of MODIS satellite data and products for monitoring air quality in the state of Texas. Atmospheric Environment 37, 2403–2412.

Hwang, H., Ro, C.U., 2006. Direct observation of nitrate and sulfate formations from mineral dust and sea-salts using low-Z particle EPMA. Atmospheric Environment 40, 3869–3880.

Huffman, G.J., Adler, R.F., Morrissey, M.M., Curtis, S., Joyce, R., McGavock, B., Susskind, J., 2001. Global precipitation at one-degree daily resolution from multi-satellite observations. Journal of Hydrometeorology 2, 36–50.

Hyslop, N.P., 2009. Impaired visibility: the air pollution people see. Atmospheric Environment 43, 182–195.

Jiang, D., Zhang, Y., Hu, X., Zeng, Y., Tan, J., Shao, D., 2004. Progress in developing an ANN model for air pollution index forecast. Atmospheric Environment 38, 7056–7064.

Jung, C.H., Cho, Y.S., Hwang, S.M., Jung, Y.G., Ryu, J.C., Shin, D.S., 2007. Analysis of measurement error for PM-10 mass concentration by inter-comparison study. Journal of Korean Society for Atmospheric Environment 23, 689–698.

Jung, J., Kim, Y.J., Lee, K.Y., Cayetano, M.G., Batmunkh, T., Koo, J.-H., Kim, J., 2010. Spectral optical properties of long-range transport Asian dust

and pollution aerosols over Northeast Asia in 2007 and 2008. Atmospheric Chemistry and Physics 10, 5391–5408

Kaimal., J.C., Wyngaard, J.C., Haugen, D.A., Cote, O.R., Izumi, Y., 1976. Turbulence structure in the convective boundary layer. Journal of the Atmospheric Sciences 33, 2152–2169.

Kalnay, E., and Coauthors, 1996. The NCEP/NCAR 40-year reanalysis project. Bulletin of the American Meteorological Society 77, 437–471.

Kim, J.Y, Ghim, Y.S., Kim, Y.P., 1999. Analysis of the present state of air pollutant emission data for the greater Seoul area. Journal of Korean Society for Atmospheric Environment 15, 813–826.

Kim, D.Y., Kim, J.W., 2000. Development of a speciated, hourly, and gridded air pollutants emission modeling system-a case study on the precursors of photochemical smog in the Seoul metropolitan area, Korea. Journal of Air and Waste Management Association 50, 340–347.

Kim, B.G., Han, J.S., Park, S.U., 2001. Transport of SO2 and aerosol over the yellow sea. Atmospheric Environment 35, 727–737.

Kim, H.S., Yi, S.M., Huh, J.B., Hopke, P.K., Holsen, T.M., 2007. Characteristics of the major chemical constituents of $PM_{2.5}$ and smog events in Seoul, Korea in 2003 and 2004. Atmospheric Environment 41, 6762–6770.

Kim, J.Y., Kim, S.-W., Ghim, Y.S., Song, C.H., Yoon, S.-C., 2012. Aerosol properties at Gosan in Korea during two pollution episodes caused by contrasting weather conditions. Asia-Pacific Journal of Atmospheric Sciences 48(1), 25–33.

Kim, K.-H., Shon, Z.-H., 2011. Long-term changes in PM_{10} levels in urban air in relation with air quality control efforts. Atmospheric Environment 45, 3309–3317.

Kim, M.-H., Kim, S.-W., Yoon, S.-C., Sugimoto, N., Sohn, B.-J., 2011. Characteristics of the lidar ratio determined from lidar and sky radiometer measurements in Seoul. Korean Meteorological Society 21, 57–67.

Kim, Y.J., Woo, J.H., Ma, Y.I., Kim, S., Nam, J.S., Sung, H., Choi, K.C., Seo, J., Kim, J.S., Kang, C.H., Lee, G., Ro, C.U., Chang, D., Sunwoo, Y., 2009. Chemical characteristics of long-range transport aerosol at background sites in Korea. Atmospheric Environment 43, 5556–5566.

Koo, Y.S., Kim, S.T., Yun, H.Y., Han, J.S., Lee, J.Y., Kim, K.H., Jeon, E.C., 2008. The simulation of aerosol transport over East Asia region. Atmospheric Research 90, 264–271. doi:10.1016/j.atmosres.2008.03.014.

Koo, Y.S., Kim, S.T., Cho, J.S., Jang, Y.K., 2012. Performance evaluation of the updated air quality forecasting system for Seoul predicting PM_{10}. Atmospheric Environment 58, 56–69.

Koo, Y.S., Yun, H.Y., Kwon, H.Y., Yu, S.H., 2010. A development of PM_{10} forecasting system. Journal of Korean Society for Atmospheric Environment 26, 666–682.

Korea National Statistical Office, Korean Statistical Information System, 2006. <http://www.nso.go.kr>.

Korean Ministry of Environment, 2007. Annual Report of Ambient Air Quality in Korea, Seoul, Korea.

Korean Ministry of Environment, 2008. Guidelines for installing and operating of air quality monitoring station.

Lau, K.-M., Ramanathan, V., Wu, G.-X., Li, Z., Tsay, S.S., Hsu, C., Sikka, R., Holben, B., Lu, D., Tartari, G., Chin, M., Koudelova, P., Chen, H., Ma, Y., Huang, J., Taniguchi, K., Zhang, R., 2008. The joint aerosol-monsoon experiment. Bulletin of the American Meteorological Society 89, 1–15.

Lee, H.I., Park, S.S., Kim, K.W., Kim, Y.J., 2008. Source identification of $PM_{2.5}$ particles measured in Gwangju, Korea. Atmospheric Research 88, 199–211.

Lee, J.H., Kim, Y.P., Moon, K.C., Kim, H.K., Lee, C.B., 2001. Fine particle measurements at two background sites in Korea between 1996 and 1997. Atmospheric Environment 35, 635–643.

Lee, K.H., Kim, Y.J., Hoyningen-Huene, W., Burrow, J.P., 2007. Spatio-temporal variability of satellite-derived aerosol optical thickness over Northeast Asia in 2004. Atmospheric Environment 41, 3959–3973.

Lee, S., Ho, C.-H., Choi, Y.-S., 2011. High- PM_{10} concentration episodes in Seoul, Korea: Background sources and related meteorological conditions. Atmospheric Environment 45, 7240–7247.

Levy, J.I., Spengler, J.D., Hlinka, D., Sullivan, D., Moon, D., 2002. Using CALPUFF to evaluate the impacts of power plant emissions in Illinois: model sensitivity and implications. Atmospheric Environment 36, 1063–1075.

Loosmore, G.A., Cederwall, R.T., 2004. Precipitation scavenging of atmospheric aerosols for emergency response applications: testing an updated model with new real-time data, Atmospheric Environment 38, 993–1003.

Murayama, T., Sugimoto, N., Uno, I., Kinoshita, K., Aoki, K., Hagiwara, N., Liu, Z.Y., Matsui, I., Sakai, T., Shibata, T., Arao, K., Sohn, B.J., Won, J.G., Yoon, S.C., Li, T., Zhou, J., Hu, H.L., Abo, M., Iokibe, K., Koga, R., Iwasaka, Y., 2001. Ground-based network observation of Asian dust events of April 1998 in East Asia. Journal of Geophysical Research 106, 18345–18359.

Nedelec, P., Thouret, V., Brioude, J., Sauvage, B., Cammas, J.P., Stohl, A., 2005. Extreme CO concentrations in the upper troposphere over northeast Asia

in June 2003 from the in situ MOZAIC aircraft data. Geophysical Research Letters 32, L14807, doi:10.1029/2005GL023141.

Niemi, J.V., Tervahattu, H., Vegkamäki, H., Kulmala, M., Koskentalo, T., Sillanpää, M., Rantamäki, M., 2004. Characterization and source identification of a fine particle episode in Finland. Atmospheric Environment 38, 5003–5012.

Noh, Y.M., Kim, Y.J., Choi, B.C., Murayama, T., 2007. Aerosol lidar ratio characteristics measured by a multi-wavelength Raman lidar system at Anmyeon island, Korea. Atmospheric Research, doi:10.1016/j.atmosres.2007.03.006.

Omar, A.H., Winker, D.M., Kittaka, C., Vaughan, M.A., Liu, Z., Hu, Y., Trepte, C.R., Rogers, R.R., Ferrare, R.A., Lee, K.P., Kuehn, R., Hostetler, C.A., 2009. The CALIPSO automated aerosol classification and lidar ratio selection algorithm. Journal of Atmospheric and Oceanic Technology 26, 1994–2014.

Park, E.S., Guttorp, P., Kim, H., 2004. Locating major PM_{10} source areas in Seoul using multivariate receptor modeling. Environmental and Ecological Statistics 11, 9–19.

Pope III, C.A., Dockery, D.W., 2006. Health effects of fine particulate air pollution: lines that connect. Journal of the Air & Waste Management Association 56, 709–742.

Qu, W.J., Arimoto, R., Zhang, X.Y., Zhao, C.H., Wang, Y.Q., Sheng, L.F., 2010. Spatial distribution and interannual variation of surface PM_{10} concentrations over eighty-six Chinese cities. Atmospheric Chemistry and Physics 10, 5641–5662.

Sakai, T., Shibata, T., Iwasaka, Y., Nagai, T., Nakazato, M., Matsumura, T., Ichiki, A., Kim, Y.S., Tamura, K., Troshkin, D., Hamdi, S., 2002. Case study of Raman lidar measurements of Asian dust events in 2000 and 2001 at Nagoya and Tsukuba, Japan. Atmospheric Environment 36, 5479–5489.

Scire, J.S., Robe, F.R., Fernau, M.E., Yamartino, R.J., 2000a. A user's guide for the CALMET meteorological model. Earth Tech, Inc., 2000, p. 332.

Scire, J.S., Strimaitis, D.G., Yamartino, R.J., 2000b. A user's guide for the CALPUFF dispersion model. Earth Tech, Inc., 2000, p. 521.

Seidel, D.J., Ao, C.O., Li, K., 2010. Estimating climatological planetary boundary layer heights from radiosonde observations: Comparison of methods and uncertainty analysis. Journal of Geophysical Research 115, D16113, doi:10.1029/2009JD013680.

Shaw, W.J., Pekour, M.S., Coulter, R.L., Martin, T.J., Walters, J.T., 2007. The daytime mixing layer observed by radiosonde, profiler, and lidar during MILAGRO. Atmospheric Chemistry and Physics Discussions 7, 15025–15065.

Shin, M.K, Lee, C.D., Ha, H.S., Choe, C.S., Kim, Y.H, 2007. The Influence of Meteorological Factors on PM_{10} Concentration in Incheon. Journal of Korean Society for Atmospheric Environment 23, 322–331.

Smith, S., Stribley, F.T., Milligan, P., Barratt, B., 2001. Factors influencing measurements of PM_{10} during 1995–1997 in London. Atmospheric Environment 35, 4651–4662.

Song, Y., Zhang, M., Cai, X., 2006. PM_{10} modeling of Beijing in the winter. Atmospheric Environment 40, 4126–4136.

Song, S.K., Shon, Z.H., Kim, K.H., Kim, K.Y., Pal, R., 2008. Dispersion and photochemical oxidation of reduced sulfur compounds in and around a large industrial complex in Korea. Atmospheric Environment 42, 4269–4279.

Stohl, A., 1996. Trajectory statistics—a new method to establish source–receptor relationships of air pollutants and its application to the transport of particulate sulfate in Europe. Atmospheric Environment 30, 579–587.

Stohl, A., 1998. Computation, accuracy and applications of trajectories—A review and bibliography. Atmospheric Environment 32, 947–966.

Stohl, A., Wotawa, G., Seibert, P., Kromp-Kolb, H., 1995. Interpolation errors in wind fields as a function of spatial and temporal resolution and their impact on different types of kinematic trajectories. Journal of Applied Meteorology 34, 2149–2165.

Stohl, A., Seibert, P., 1998. Accuracy of trajectories as determined from the conservation of meteorological tracers. Quarterly Journal of Royal Meteorological Society 124, 1465–1484.

Sun, J., Zhang, M., Liu, T., 2001. Spatial and temporal characteristics of dust storms in China and its surrounding regions, 1960– 1999: Relations to source area and climate. Journal of Geophysical Research 106, 10,325–10,333, doi:10.1029/2000JD900665.

Sung, H., Oh, J.T., 2011. Transit-oriented development in a high-density city: Identifying its association with transit ridership in Seoul, Korea. Cities 28, 70–82.

Uno, I., Eguchi, K., Yumimoto, K., Takemura, T., Shimizu, A., Uematsu, M., Liu, Z.Y., Wang, Z.F., Hara, Y., Sugimoto, N., 2009. Asian dust transported one full circuit around the globe. Nature Geoscience 2, 557–560.

Van Der Wal, J.T., Janssen, L.H.J.M., 2000. Analysis of spatial and temporal variations of PM_{10} in the Netherlands using KALMAN filtering. Atmospheric Environment 34, 3675–3687.

Vardoulakis, S., Kassomenos, P., 2008. Sources and factors affecting PM_{10} levels in two European cities: Implications for local air quality management. Atmospheric Environment 42, 3949–3963.

Winker, D.M., J. Pelon, J.A. Coakley, Jr., S.A. Ackerman, R.J. Charlson, P.R. Colarco, P. Flamant, Q. Fu, R. Hoff, C. Kittaka, T.L. Kubar, H. LeTreut, M.P. McCormick, G. Megie, L. Poole, K. Powell, C. Trepte, M.A. Vaughan, B.A. Wielicki, 2010. The CALIPSO Mission: A global 3D view of aerosols and clouds, Bulletin of the American Meteorological Society 91, 1211-1229, doi: 10.1175/2010BAMS3009.1.

Xie, C., T. Nishizawa, N. Sugimoto, I. Matsui, and Z. Wang, 2008. Characteristics of aerosol optical properties in pollution and Asian dust episodes over Beijing, China. Applied Optics, 47, 4945–4951.

Yang, D., Han, Y., Gao, J., The, J., 2007. Transport of airborne particulate matters originating from Mentougou, Beijing, China. China Particuology 5, 408–413.

Yi, S.M., Lee, E.-Y., Holsen, T.M., 2001. Dry deposition fluxes and size distribution of heavy metals in Seoul, Korea during yellow-sand events. Aerosol Science and Technology 35, 569–576.

Yoon, S.-C., Y.-J. Lee, S.-W. Kim, M.-H. Kim, and N. Sugimoto, 2010. Measurements of the lidar ratio for Asian dust and pollution aerosols with a combined Raman and back-scatter lidar. Atmosphere. Korean Meteorological Society 20, 483–494.

Zhang, Q., Streets, D.G., Carmichael, G.R., He, K.B., Huo, H., Kannari, A., et al., 2009. Asian emissions in 2006 for the NASA INTEX-B mission. Atmospheric Chemistry and Physics 9, 5131–5153.

국문초록

서울시에서는 대기질을 개선하기 위해 천연가스버스 도입, 자동차 배출저감장치 부착, 연료 질 개선 등 지난 수 년 간 다각적인 노력을 기울인 결과, 직경 10 μm 이하인 미세먼지(PM_{10})의 경우 그 농도가 약 70 μg m^{-3} 이었던 2000년대 초에 비해 2012년 기준 약 50 μg m^{-3} 까지 개선되는 성과를 거두었다. 그러나 여전히 선진국의 대도시에 비해서는 상당히 높은 수준이며 대기환경기준(일평균 미세먼지 농도 100 μg m^{-3} 미만)을 초과하는 PM_{10} 고농도 현상 역시 빈발하고 있다. 본 연구에서는 최근 서울 지역에서 PM_{10} 고농도 현상이 나타났던 사례를 중심으로 대기오염물질의 발원지역과 이동 경로를 조사하여 외부적 영향의 기여도를 파악하는 한편, 관련된 기상장을 분석하여 대기오염물질의 장거리 이동을 유발하고 고농도 현상을 유지시키는 기상 조건을 밝히고자 하였다.

2001년부터 2008년까지의 기간 동안 PM_{10} 고농도 현상이 발생한 총 254일에 대하여 기류 역궤적 분석을 수행하여 고농도 PM_{10}의 발원 지역과 이동 경로를 분석한 결과, PM_{10} 고농도 사례는 외부에서 이동해온 대기오염물질의 영향을 받은 사례(176일)와 국지적인 배출에 의해 발생한 사례(78일)로 분류되었다. 외부의 미세먼지 발원 지역은 주로 인위적 에어러솔의 배출이 많은 공업 지역 및 대도시가 위치한 중국 북동부 지역과 자연적 에어러솔의 배출이 많은 고비 사막 주변이었다. 발원 지역에 따른 PM_{10} 고농도 사례 타입 별로 기상장 합성 분석을 수행한 결과, 특정한 기압 배치와 이에 동반된 기류 패턴에 의해 발원 지역에서의 대기오염물질의 상승 및 이동, 한국 지역에서의 오염물질 낙하 및 축적 등이 이루어져 PM_{10}

고농도 현상이 발생하는 것으로 추정된다.

PM_{10} 고농도 현상의 발생 및 유지 기작을 더욱 면밀하게 파악하기 위하여 최근의 대기질 개선에도 불구하고 이례적으로 오랜 기간 유지되었던 2008년 10월의 PM_{10} 고농도 사례에 대하여 지상 및 원격 관측 자료 분석, 기류 역궤적 분석 및 발원 지역의 PM_{10} 농도 변화 분석, 대기 확산 모델링 분석 등을 수행하였다. 위성으로부터 관측된 에어러솔 광학 두께의 수평 분포 자료와 에어러솔 및 구름의 연직 분포 자료, 기류 분석 결과를 통해 중국 지역으로부터 한국 지역으로의 에어러솔의 이동을 관찰할 수 있었고, 종관 일기도 분석과 하층 대기 안정도 분석을 통해 특정한 기압 패턴과 이에 동반된 기류의 흐름이 발원 지역에서의 에어로솔의 상승 및 이동, 한국 지역에서의 안정적인 하층 대기 조건을 형성하여 PM_{10} 고농도 현상의 발생 및 유지에 결정적인 역할을 하는 것으로 파악되었다. 관측 자료 분석에 의해 밝혀진 월경성 오염물질의 이동과 PM_{10} 고농도 현상 유지 기작은 기류 역궤적 모델링 및 대기 확산 모델링을 통해서도 확인되었다. 본 연구에서 논의한 한국 지역에서 발생한 PM_{10} 고농도 현상의 발원 지역과 이동 경로 및 관련 기상장에 대한 연구 결과들은 미세먼지 배출 조절 정책 및 대기오염물질의 장거리 이동에 대한 동아시아 국가들의 협력에 과학적인 근거가 될 것으로 기대한다.

주요어: 미세먼지, 월경성 대기오염물질, 발원지역, 이동경로, 기상조건

학번: 2008-30821